1.0

.28   2.5

3.2   2.2

2.0

1.1

1.8

1.25   1.4   1.6

MICROCOPY RESOLUTION TEST CHART

RADC-TR-81-372, Vol I (of two)
Final Technical Report
January 1982

AD-A111481-V2

TOPICS IN OPTICAL MATERIALS AND DEVICE RESEARCH - II

Parke Mathematical Laboratories

T. B. Barrett
H. Haskel
C. E. Ryan
R. V. Wood
S. P. Yukon

DTIC
SELECTE
MAR 2 1982
H

ROME AIR DEVELOPMENT CENTER
Air Force Systems Command
Griffiss Air Force Base, New York 13441

82 03 02 027

This report has been reviewed by the RADC Public Affairs Office (PA) and is releasable to the National Technical Information Service (NTIS). At NTIS it will be releasable to the general public, including foreign nations.

RADC-TR-81-372, Vol I (of two) has been reviewed and is approved for publication.

APPROVED: *Carl H. Pitha*

CARL PITHA
Project Engineer

APPROVED: *Freeman D. Shepherd*

FREEMAN D. SHEPHERD, JR.
Acting Director
Solid State Sciences Division

FOR THE COMMANDER: *John P. Huss*

JOHN P. HUSS
Acting Chief, Plans Office

If your address has changed or if you wish to be removed from the RADC mailing list, or if the addressee is no longer employed by your organization, please notify RADC.(ESO) Hanscom AFB MA 01731. This will assist us in maintaining a current mailing list.

Do not return copies of this report unless contractual obligations or notices on a specific document requires that it be returned.

REPORT DOCUMENTATION PAGE		READ INSTRUCTIONS BEFORE COMPLETING FORM
1. REPORT NUMBER RADC-TR-81-372, Vol I (of two)	2. GOVT ACCESSION NO. AD-A111762	3. RECIPIENT'S CATALOG NUMBER
4. TITLE (and Subtitle) TOPICS IN OPTICAL MATERIALS AND DEVICE RESEARCH - II		5. TYPE OF REPORT & PERIOD COVERED Final Technical Report 1 Apr 78 - 30 Sep 80
		6. PERFORMING ORG. REPORT NUMBER N/A
7. AUTHOR(s) T. B. Barrett R. V. Wood H. Haskel S. P. Yukon C. E. Ryan		8. CONTRACT OR GRANT NUMBER(s) F19628-78-C-0089
9. PERFORMING ORGANIZATION NAME AND ADDRESS Parke Mathematical Laboratories 1 River Road Carlisle MA 01741		10. PROGRAM ELEMENT, PROJECT, TASK AREA & WORK UNIT NUMBERS 62702F 46001927
11. CONTROLLING OFFICE NAME AND ADDRESS Deputy for Electronic Technology (RADC/ESO) Hanscom AFB MA 01731		12. REPORT DATE January 1982
		13. NUMBER OF PAGES 90
14. MONITORING AGENCY NAME & ADDRESS(if different from Controlling Office) Same		15. SECURITY CLASS. (of this report) UNCLASSIFIED
		15a. DECLASSIFICATION/DOWNGRADING SCHEDULE N/A

16. DISTRIBUTION STATEMENT (of this Report)

Approved for public release; distribution unlimited.

17. DISTRIBUTION STATEMENT (of the abstract entered in Block 20, if different from Report)

Same

18. SUPPLEMENTARY NOTES

RADC Project Engineer: Carl A. Pitha (ESO)

19. KEY WORDS (Continue on reverse side if necessary and identify by block number)

Fiber-Optics	Optical Time-Domain Reflectometry	Nicolet
Optical Waveguide	Computer	
Wavelength Multiplexing	Silicon	Optical Pulse Generator
CCD	Silicon Nitride	88
Crystal-Growth Mechanism	Silicon Dioxide	

20. ABSTRACT (Continue on reverse side if necessary and identify by block number)

1. A new analysis of fiber-optic wavelength multiplexing was developed.
2. A study of the limitations imposed by materials quality on CCD's was carried out.
3. The SiO_2-Si interface and its problems were investigated.
4. Epitaxial growth mechanism for silicon, silicon nitride, and silicon dioxide were studied.
5. A theory was developed to describe time-domain reflectometry return signals.

DD FORM 1473 EDITION OF 1 NOV 65 IS OBSOLETE

signals.

Foreword

This report is the first part of a two-part final report for Contract F19628-78-C-0089. Part II, dealing with the construction and operation of a IEEE-488 (GPIB) interface for the Nicolet 1080 computer is entitled: *GPIB Interface for the Nicolet 1080 Computer.*

The following individuals have contributed to results reported on in these reports.

        Laurence Armour - Consultant to PML
        Dean Bandes - Parke Mathematical Laboratories
        Theodore B. Barrett - Parke Mathematical Laboratories
        George Bartley - Consultant to PML
        Carl Cioffi - Parke Mathematical Laboratories
        Arthur Harrison - Parke Mathematical Laboratories
        Haim Haskal - Consultant to PML
        Charles Ryan - Consultant to PML
        Ralph Van Wood - Consultant to PML
        Stanford Yukon - Consultant to PML

iii

TABLE OF CONTENTS

<u>Preface</u> (to Part I)

This report, composed of four sections, provides a summary of
work accomplished under this contract in four diverse areas of
optical transmission and processing. Briefly, these sections
consist of:

I. A description of optic of wavelength multiplexing. This
   section includes as an attachment a report on the subject
   presented at the Conference on the Physics of Fiber Optics
   (Chicago, April 1980).

II. A summary of techniques for the fabrication of charge coupled
    devices (CCD); with emphasis on the selection and evaluation
    of wafers, oxidation of wafers and the preparation of fibers
    on the oxidized wafers.

III. A short summary of work which was done on the development of a
     device to produce short duration, high energy optical pulses.

IV. The theoretical development of optical time domain reflecto-
    metry applied to optical waveguides with weak static perturba-
    tions. This section also includes as an attachment a report
    on the subject presented at the Chicago Conference.

Other work for this contract was done to enhance the collection
and evaluation of data on optical properties of various solid
state materials. This work included both the development of
hardware and software devices for this purpose. Part II of this
report describes the hardware and software which was developed to
interface a Nicolet 1080 computer to the GPIB (IEEE-488)
specifically for use with a video camera with digital output (via
thE GPIB). Other work in this area has been previously reported
on in various quarterly status reports and Technical Memoranda.
Briefly, this work consisted of:

(1) The construction of a data encoder for use with various
    spectrometers with analog output. This encoder is used with
    a Sykes Comm-Stor (Communications/Storage) unit to create
    files of data which are later transferred to the CDC6600 and
    analyzed using softare created for a Digilab FTS-14 spectro-
    meter (see Final Report RADC-TR-78-61 for details of the
    FTS-14 software).

(2) Revision of the FTS-14 data reduction and analysis software
    for use with various signal sources including the above
    mentioned encoder. This revised software is used with output
    from the data encoder, a punched paper tape recorder as well
    as the FTS-14.

(3) Investigation into the generation of correlation masks using the AFGL CRT plotter. This included the generation of resolution test strips and corrected resolution test strips based on correction coefficients found from the uncorrected strips. In addition, assembly language programs were developed for the Nicolet computer to test the feasibility of using this device to generate correlation masks in real time.

(4) A set of software tools for signal processing and display, labeled collectively as SIGPRODS, was modified for use with parametric plots. This is specifically used with software which is used to model the operation of a class of tunable lasers.

SECTION I

Fiber Optic Wavelength Multiplexers

During the duration of this contract we concentrated our efforts on developing new concepts for fiber optic wavelength multiplexers.

In particular we were interested in devices which are easy to fabricate and thus economical and which display low insertion loss. This led us to the idea that one could devise a single element multiplexer. The literature on multiplexers, not a very extensive one, was searched. Basically, multiplexers utilize two elements: a focussing-collimating lens and a dispersive element. The dispersive element can take the form of a prism but preferably a diffraction grating to keep the size of the device small. One can also utilize for channel separation a number of narrow band interference filters arranged in a structure which allows separating the various channels (optical carriers) at different output ports.

The concept of a single-element multiplexer triggered our interest in Fresnel Zone Plates (FZP) because FZP's act as focussing diffraction gratings and have high dispersive power.

The focal length of a FZP is inverse proportional to wavelength. Let the focal length be f_0 at a wavelength of λ_0 at an arbitrary wavelength λ, we have

$$f(\lambda) = f_0 \frac{\lambda_0}{\lambda} \tag{1}$$

Taking the logarithmic derivative of (1), we obtain

$$\frac{df}{f} = -\frac{d\lambda}{\lambda} \tag{2}$$

And thus the axial separation between two adjacent channels is

$$\Delta f = f \frac{|\Delta\lambda|}{\lambda} \tag{3}$$

where $\Delta\lambda$ is the interchannel separation, typically 20-30nm.

On the question of low insertion loss of the demultiplexer, one must be careful to select the proper type of FZP.

A "black-and-white" FZP consisting of alternative opaque and transparent zones has a maximum efficiency of 10%, that is, it introduces an insertion loss of 10dB.

A phase reversal FZP, in which all zones are transparent but they introduce a differential phase retardation of π between adjacent zones, has a maximum efficiency of 40%, i.e., an insertion loss of 6dB.

One can do better by utilizing a phase Fresnel lens or as it has been recently designated, a blazed Fresnel Zone Plate (BFZP). Such a device is capable of the dispersion given by equations (1)-(3) but introduces negligible insertion loss over a 20% bandwidth.

The real problem that remains to be solved is to find a good method for fabricating a BFZP. Interest in BFZP exists also in the X-ray field where it can be used as an efficient lens. By holographic methods one can create FZP's which are highly efficient in materials such as dichromated gelatin. The problem is that most of the interest in fiber optics is in the near infrared portion of the spectrum where no known materials exist for holography. To circumvent this problem, one can create the FZP's with an argon laser at a visible wavelength, say $\lambda = 0.515\mu$m and playback in the IR. Work remains to be done to reduce the aberrations which occur when a hologram is made at one wavelength and played back at a different wavelength.

A paper on the Fresnel Zone Plate demultiplexers by Haim Haskal has been presented at the Conference on the Physics of Fiber Optics in Chicago on April 28, 1980. The full paper is scheduled to appear in the proceedings of the conference.

4

SECTION II

Charge Coupled Device Fabrication Steps

I. INTRODUCTION

During the contract period my effort has related largely to the preparation and processing of silicon wafers to be used in the fabrication of experimental charge coupled devices (CCD)[1] For the most part this work has involved day to day contact with members of ESE, particularly Mr. Irvin Berman. Periodic written reports (quarterly) and special oral and written reports have been submitted to PML and the Contract Monitor.

Major emphasis has been on the selection and evaluation of wafers, the oxidation of wafers, and the preparation of films of polycrystalline silicon and Silicon Nitride on the oxidized wafers.

Along with the day to day laboratory type activities, literature surveys and evaluations, somehwat in the form of annotated bibliographies, have been made. These studies include:

a) Limitation imposed on CCD's due to the quality of available silicon wafers.
b) Problems related to the SiO_2/Si interfaces.
c) Front side and back side lettering techniques.
d) Expetaxial growth mechanisms for polycrystalline silicons, silicon nitride (Si_3N_4) and low temperature silicon dioxide (SiO_2) layers.
e) New technology that may impact CCD.

These literature surveys (together with copies of almost all the articles referred to therein) are available in ESE. In this report we are merely summarizing some of the conclusions and/or recommendations that have evolved from the combination of the laboratory activities and the current literature studies. These recommendations and conclusions are specific to the specialized ESE environment where it is desired to make sample quantities of research devices at or beyond the present state of the art. The referneces given in this report are for the most part quite general and are for background to the specific area rather than justification for the conclusions.

II. LIMITATIONS IMPOSED ON CCD DUE TO THE QUALITY OF THE WAFER USED

1. There is little liklihood that any material will replace silicon as the semiconductor from which CCD's are made. Hess and Sah[2] show that the higher mobilities of less tightly bonded semiconductors (e.g., III-V Compounds) cannot be effectively used because of the saturation of the drift velocity of the electrons and the hot electron effects in the fringing fields inherent in the CCD geometry. Jastrzebski[3] shows that deep recombination centers are the limiting crystal defect in silicon CCD devices. These types of defects are far more numberous in compound semiconductors. Hence this report will discuss silicon only.

2. Charge Coupled Devices are extremely sensitive to defect introduced both in the silicon growth procedures and in the processing steps applied to the silicon wafers prepared from the grown crystals. Hence the problems for achieving the objectives of Very Large Scale Integration (VLSI) and Very High Speed Integration (VHSI) are closely related to the corresponding problems in CCDS. Specifically, these objectives are higher density of smaller elements on larger chips, higher speed, greater reliability, higher yields and lower costs.

3. The rapid progress made in the last few years on the objectives cited above have been largely due to improvements in the processing steps on the wafers. There has been considerable discussion and difference of opinion on whether or not the present quality of crystals grown by the Czochralski or Float Zone technique are adequate to meet the needs of submicrometer size devices. Stated another way, the question is as follows: can improvements (lower temperatures) in the processing steps and gettering and annealing techniques compensate adequately for the defects in the "as grown" crystals?

   First we will briefly summarize the crystal growth situations. Practically all of the research and development on production and experimental devices utilize dislocation free Czochralski (CZ) or Float Zone (FZ) crystals. Consequently, we will confine our attention to these forms of silicon crystal growth.

   The CZ crystals have the advantages of higher physical perfection, ready availability and better cost and yield factors. The FZ crystals have greater chemical purity but suffer higher levels of physical imperfections. The greater chemical purity of the FZ crystals is due to the elimination of the quartz crucible and carbon susceptors and resistance heaters which are the principal source of oxygen and carbon impurities in the CZ process. The greater physical perfection of the CZ crystals is due to a larger melt in which the thermal convection currents are better controlled. Extensive discussions of the status of CZ and FZ growth, the effects of oxygen and

carbon and the types and nature of crystal defects are given
in publications of the Electrochemical Society[4] and the
International Conference on Crystal Growth (ICCG)[5]. An
excellent review of the limitations imposed on the CZ growth
by thermal convection effects has been published by J.R.
Carruthers[6] and by Carruthers and Witt[7]. A similar review
emphasizing FZ crystals has been published by deKock[8]. These
publications and a large number of current papers adequatley
attest to the difficulty of improving either of these types of
crystal growths (CZ or FZ). A summary of selected properties
of single crystal silicon together with the present capabili-
ties and requirements for VLSI is given in Table I which is
taken from Bullis[9]. This table is originally from a report,
as yet unpublished, by a select committee of The National
Academy of Science[10]. The table clearly shows the need for
improvements of a factor of ten or better in many cases. Such
improvements are unlikely in the near future in large diameter
crystals.

TABLE I

Selected Properties of Single-Crystal Silicon

Property	Current Capabilities		Requirements
	Czochralski	Float Zone	for VLSI
Resistivity n-type (P), $\Omega \cdot cm$	1-40	1-300	100-400
Resistivity n-type (Sb), $\Omega \cdot cm$	0.005-10		0.0002-0.02
Resistivity p-type (B), $\Omega \cdot cm$	0.005-50	1-300	100-400
Resistivity gradient (four-probe) %	5-10	20	<1
Resistivity microsegregation, %	10-15	20-50	<1
Minority carrier lifetime, s	30-300	50-500	300-1000
Oxygen, ppma	5-15	Not detected	Uniform and controlled
Carbon, ppma	1-5	0.1-1	0.1
Heavy-metal impurities, ppba	1	0.01	0.001

The conclusion from a fairly extensive study of many of these
factors is simply that ESE should continue to use wafers of ≤ 2
inches in diameter with a strong preference for FZ crystals. The
smaller diameters allow much greater crystal perfection due to
much better control of convection factors. The FZ crystals,
despite larger resistivity striations have much smaller varia-
tions in generation lifetime. This is in turn due to the lower
level of deep recombination centers made possible by reduction of
oxygen and carbon in FZ crystals.

4. Since the number of wafers used in an experimental program is quite small, and the research time spent per wafer is high, the cost per wafer is relatively insignificant. Hence one should acquire the best possible pedigreed wafers to the most exacting specifications.

   The incoming wafers should be extensively tested on a sample basis and processed ins small batches of the order of ten at a time. The desirable incoming tests are a) X-ray topography, b) Phase Contrast microscopy on "Secco" etched wafers and c) Capacitance-voltage measurements (C-V). All three of these tests are time consuming and the latter two are destructive as well (i.e., further processing steps would be required before reusing the wafer). Nevertheless, physical tests like (a) and (b) are essential, as well as electrical tests like (c) in order to correlate electrical properties of the experimental devices with physical and chemical properties of the wafer. ESE has excellent capability for all three of these tests.

5. What is really needed is a rapid, non-destructive imaging technique that would put a high resolution image of the defect pattern of a wafer onto a cathode ray tube. The best approach[11],[12] to this type of device is to use laser scanning beams to measure surface and interface properties of wafers before and after various process steps. DiStefano's device has been developed with partial support of government funds. Such a piece of measuring equipment would be a great asset to ESE.

   Bullis[9] has written an excellent review of methods of characterizing semiconductor material. Another excellent recent review of the present status of silicon for electronic devices is given by Bradshaw and Goorissen[13].

   It is strongly recommended that Dr. W. Murray Bullis (National Bureau of Standards) be consulted both on the appropriate wafer tests and on acceptable sources of wafers.

III. PROBLEMS RELATING TO SILICON OXIDATION

Having selected and prepared the wafer, the next step is to put onto it a layer of the order of 0.1 to 1.0 micron (1000 to 10,000 A°) of silicon dioxide (S_iO_2). The current accepted practice is to use a dry thermal oxidation at a temperature of the order of 1000C°. The time and temperature cycle for these oxidations is such that many defects native to the wafer are developed and many more may be introduced in this processing step. Furthermore, the properties of the interface between the silicon and the silicon dioxide layer (Si/S_iO_2) often varied widely. These properties (fixed Oxide Charges O_f and N_f) are very important in many CCD devices.

Because of inadequate knowledge of the oxidation mechanism, the physics and chemistry of the Si/SiO_2 interface, the effects of thermal annealing on the defect structure and inconsistency in definitions and nomenclature, it was difficult to follow and evaluate much of the copious literature in this area. The situation is now becoming much clearer. The nomenclature and definition problem has been clarified by Deal and his Committee[14]. The Si/SiO_2 interface problems are reviewed in a comprehensive way in the Proceedings of the International Conference on the Physics of SiO_2 and Its Interfaces[15]. The understanding of the roles of chlorine[16] and hydrogen[17] in frontside gettering has permitted much more consistent data. Backside gettering[18] is a technique wherein purposely introduced imperfections (dislocations) in the inactive portion of the silicon wafer act as sinks to remove imperfections and impurities from the critical active device regions of the wafer. This technique (backside gettering) is probably the largest single advance in device processing introduced in the last several years in terms of increased yield and quality of devices.

The combination of frontside gettering (using chlorine), backside gettering (using phosphorous diffusion) and controlled annealing should allow the processing of excellent SiO_2 layers with superior Si/SiO_2 interfaces onto excellent quality substrates.

The particular implementation of these techniques depends on the circumstances of the particular group involved. The particular recommendations for ESE are as follows:

a) The backside gettering, using the phosphorous diffusion technique of Rozgonyi[18] is preferred. ESE has also the capability for backside gettering by ion implantation and/ or mechanical abrading (sand blasting).

b) The frontside gettering technique of Hattori[19],[20] which uses a $N_2/HCl/O_2$ preoxidation anneal is preferred. However, Trichlorethylene (TCE)[21] should be used in place of HCl as it is less corrosive and easier to handle. One significant advantage of this preoxidation anneal is that it is done "in situ" immediately prior to the oxidation and acts as a final cleaning step for the wafer. The importance of the proper combination of frontside gettering, backside gettering and slow annealing on the defect structure of Float Zone wafers is clearly shown by Rohatgi and Rai-Choudhury[22]. Their technique, which can be readily combined with that of Hattori yields millisecond carrier lifetime measurements which are indicative of very high quality defect free wafers. These combined techniques applied to two inch diameter Float Zoned wafers should provide high quality oxide layers with good interface properties and potentially excellent CCD device properties (low leakage, etc.).

IV. DEPOSITION OF POLYSILICON LAYERS

The preparation of thin films of semiconductors onto substrates of identical composition (epitaxy) and onto substrates of different composition (hetero-epitaxy) by Chemical Vapor Deposition (CVD) techniques has increased very rapidly over the past decade and it can easily be predicted that this trend will continue for many years to come. There are several reasons for this situation:

a) The planar technology has required relatively thin active layers with precisely controlled properties. The drives toward VLSI and VHSI sharply accentuate the importance of thin high quality layers (usually in the region of 100 to 1000 A^{o}).

b) CVD is an extremely versatile technique with a very wide range of applications for elemental and compound semi-conductors, conductors, resistors, and capacitative components.

c) The cost and complexity of setting up an epitaxial system is far less than to set up a Czochralski or Float zone facility.

d) There are very many opportunities for practical application investigations as well as fundamental investigations of CVD processes. In other words, the potential field for new research opportunities is much larger and the state of the art is far less developed than that of growth from the melt.

e) There are very many investigations that are suitable for doctoral theses in universities without excessive investment in capital equipment. The individuals thus trained are highly desirable in small and specialized, as well as large and generalized industrial organizations.

f) New epitaxial techniques will probably replace many presently used processing steps (see Section V of this report - New Technologies).

There are a number of excellent reviews on the subject of Chemical Vapor Deposition of semiconductors[23] and particularly of silicon[24]. Our attention has been confined to the deposition of polysilicon by CVD with emphasis on low pressure CVD (LPCVD) and plasma enhanced CVD (PECVD).

The advantages of LPCVD are clearly spelled out by Hammond[23]. He outlines a simplified barrier layer theory in which he shows that the diffusion rates for the gaseous species are inversely proportional to the total system pressure and directly proportional to the partial pressure of the gaseous species in the mainstream. Also the diffusion rate is directly proportional to temperature to the three-halves power ($T^{3/2}$). Thus, by reducing pressure from one atmosphere to a fraction of a TORR, the

10

diffusion rate is increased by a factor of about a thousand while
the deposition rate is reduced very little since no dilutent
gases are used. Thus, the uniformity of the deposited layers is
greatly enhanced, within the individual wafers, from wafer to
wafer, and from batch to batch. The merits and details of LPCVD
are discussed by Rossler[24], by Ogirima et al[25], and by Spear
and Wang[26].

The specific applications of LPCVD for ESE are discussed in an
internal report[27]. This report discusses two LPCVD systems.
One of these is essentially a "turn key" retrofit system to be
installed on the ESE Lindberg furnace. The other is an "in
house" experimental system which is scaled down for specific
needs. Operation of the first system is now scheduled for April
1981. The second system is currently being "debugged".

It is recognized that Plasma Enhanced CVD systems (PECVD) may
have many advantages over LPCVD systems. However, they also have
additional compilations so that there will be little emphasis in
ESE on PECVD until after the LPCVD is fully implemented. It is
the present intent to use a system which is a modification of
that Rosler and Engle[28]. The current thinking concerning the
proposed system is discussed in the internal report cited[27].
It represents a conversion of the present MiniPak II system to an
R.F. Heated Hot Wall system.

V. NEW TECHNOLOGIES THAT MAY INFLUENCE NEW CCD DEVICES

Some effort has been expended in exploring new technologies that
may influence future directions of VLSE, VHSI and CCD research.
They will merely be mentioned here. The most significant trend
in my opinion is the increasing significance of Chemical Vapor
Deposition. A good part of the recent success has related to
better control of the variables involved and to higher purity
intermediate starting materials such as $SiCl_4$, $SiHCl_3$ and SiH_4.

The major limitations of CVD has been the substrates. The possi-
bilities of reusing substrates by cleaving the epilayers, the use
of contoured foreign substrates (graphoepitary) and the use of
laser, electrons and ion beam annealing of epitaxial layer or
foreign substrates may radically change our current processing
technologies in the next decade. The ability to deposit SiO_2
layers by CVD techniques whose properties are comparable or
superior to thermal SiO_2 is apparently possible[29].

Despite theoretical arguments that ideal SiO_2-Si interfaces are
possible[30], it is unlikely, in my opinion, that the fixed
charge density at the SiO_2/Si interface will be reduced much
below the present best values of the order of $10^{10} cm^{-2}$. Despite
the central importance that SiO_2 has had on the development of

11

our current electronic devices and systems, it may be necessary to develop a new insulating interface with appropriate crystallographic, as well as thermal and mechanical properties if we are to greatly improve on present interface conditions and to make truly three-dimensional (layered) VLSI and VHSI devices. One possibility would be magnesium Spinel $MgAl_2O_4$ if it could be deposited on silicon substrates in single crystal form by metaloorganic techniques. Then multiple alternate layers of single crystal silicon and spinel could be used to explore the feasibility and desirability of truly three-dimensional devices.

The rapid development of computer aided design and computer aided manufacturing techniques (CAD/CAM) will greatly accelerate new VLSE, VHSI and CCD design and prototype chips at greatly reduced cost.

VI.   FUTURE DIRECTIONS

It is anticipated that next year's efforts will be much more restricted in scope and relate the experimental aspects of the LPCVD and PECVD programs.

REFERENCES

(1)   R.W. Brodersen and R.M. White, "Charge Transfer and Surface
      Acoustic Wave Techniques", Advances in Electronics and
      Electron Physics, L. Marton and C. Marton, Eds. Vol 51
      (1980) pp.265-308.
(2)   K. Hess and C.T. Sah, "The Ultimate Limits of CCD
      Performance Imposed by Hot Electron Effects", Solid State
      Electronics Vol 22 (1979) pp.1025-1033.
(3)   L. Jastrzebski, P. Levine, A. Cope, W. Henry and D. Battson,
      "Material Limitations Which Cause Striations in CCD
      Imagers", IEEE Transactions on Electron Devices, Vol ED-27
      No.8 August 1980 pp.1694-1701.
(4)   "Semiconductor Silicon-1977", Electrochemical Society
      Proceedings Vol 77-2.
(5)   R. Ureda and J.B. Mullin, Eds., "Crystal Growth and
      Characterization", North-Holland Publishing Co. (1975)
(6)   J.R. Carruthers, "Thermal Convection Instabilities Relevant
      to Crystal Growth From Liquids", Preparation and Properties
      of Solid State Materials, Wilcox and Lefever, Eds., Marcel
      Dekker, Inc. pp.1-121.
(7)   J.R. Carruthers, A.F. Witt and E. Reusser, "Czochralski
      Growth of Large Diameter Silicon Crystals - Convection and
      Segregation", Silicon-1977 Loc.cit. p.61.
(8)   A.J.R. deKock, "Effect of Growth Conditions on Semiconductor
      Crystal Quality", Current Topics in Material Science - 1976
      Crystal Growth and Materials, E. Kaldis and H. Scheel, Eds.,
      North Holland Publishing Co. (1977) pp.661-704.
(9)   W. Murray Bullis, "Characterizing Semiconductor Materials",
      Semiconductor International, Oct. 1980 pp.79-91.
(10) Panel on Thin Film Microstructure Science and Technology,
      National Academy of Sciences, 1979.
(11) T.H. DiStephano and J.M. Viggiano, "Interface Imaging by
      Scanning Internal Photoemission", IBM Journal of Research
      and Development Vol 18, No.2 March 1974 pp.94-99.
(12) J.C. White, T.F. Unger and J.G. Smith, "Contactless
      Nondestructive Technique for Diffusion Length in Silicon",
      Solid State and Electron Devices, Sept 1977, Vol 1, No.5
      pp.139-145.
(13) S.E. Bradshaw and J. Goorissen, "Silicon for Electronic
      Devices", Journal of Crystal Growth 48 (1980) pp.514-529.
(14) B.E. Deal, "Standardized Terminology for Oxide Charges
      Associated with Thermally Oxidized Silicon", IEEE
      Transactions on Electron Devices, Vol ED-27, No.3 March 1980
      pp.606-608.
(15) S.T. Pantelides, Ed., "The Physics of SiO_2 and its
      Interfaces", Pergamon Press 1980.

(16) J. Monkowski, "Role of Chlorine in Silicon Oxidation", Part
      I Solid State Technology, July 1979, Part II August 1979.
(17) A.G. Revesz, "Hydrogen in SiO_2 Films on Silicon", see Ref.
      15, pp.222-226.
(18) G.A. Rozgonyi et al, "Elimination of Oxidation Induced
      Stacking Faults by Preoxidation Gettering of Silicon
      Wafers";
      I. "Phosphorous Diffusion-Induced Misfit Dislocations",
      Journal of Electrochemical Soc. Vo. 122 No.12 Dec. 1975;
      II. "Si_3N_4 Process", Ibid Vol 123 No.4 April 1976;
      III. "Defect Etch Pit Correlation with P-N Junction
      Leakage", Ibid Vol 123 No.4 April 1976.
(19) T. Hattori and T. Suzucki, "Elimination of Stacking Fault
      Formation in Silicon by Preoxidation in $N_2/HCl/O_2$ Mixtures",
      App. Phys. Lett. 33(4) 15 August 1978.
(20) T. Hattori, "Gettering of Stacking-Fault Nuclei in Silicon
      by use of HCl", Semiconductor International, July/August
      1979.
(21) T. Hattori, "TCE Oxidation for the Elimination of
      Oxidation-Induced Stacking Faults in Silicon", Solid State
      Technology, Nov. 1979.
(22) A. Rohatgi and P. Rai-Choudhury, "Process Induced Effects on
      Carrier Lifetime and Defects in Float Zone Silicon", Journal
      of Electrochemical Soc., Vol 127 No.5 May 1980.
(23) M.L. Hammond, "Introduction to Chemical Vapor Deposition",
      Solid State Technology, Dec. 1979 pp.61-65.
(24) R.S. Rossler, "Low Pressure CVD Production Processes for
      Poly, Nitride and Oxide", Solid State Technology, April 1977
      pp.63-70.
(25) M. Ogirima, H. Saida, M. Suzuki and M. Maki, "Low Pressure
      Silicon Epitaxy", Journal of Electrochemical Soc., Vol 124
      No.6 June 1977 pp.903-908.
(26) K.E. Spear and M.S. Wang, "Thermochemical Calculations on
      the LPCVD of Si_3N_4 and SiO_2", Solid State Technology, July
      1980 pp.63-68.
(27) C.E. Ryan, "Recommendations for Low Pressure Chemical Vapor
      Deposition (LPCVD) Program", dated 8 January 1980.
(28) R.S. Rosler and G.M. Engle, "LPCVD-Type Plasma-Enhanced
      Deposition System", Solid State Technology, Dec. 1979
      pp.88-92.
(29) L.A. Kasprzak and A.K. Gaino, "Neat-Ideal $Si-SiO_2$
      Interfaces", IBM Journal of Research and Development, Vol 24
      No.3 May 1980 pp.348-352.
(30) R.B. Loughlin, J.D. Joannopoulos and D.J. Chadi, "Electronic
      Structure of the $Si-SiO_2$ Interface", see Ref. 15 pp.
      321-327.

SECTION III

Generation of Short, High-Energy Pulses

During this period, a major effort was directed toward develop-
ment of a circuit to produce repetitive, short, high-energy
optical pulses. The initial design goal was an optical pulse
duration of about 10 ns. Given sufficient energy per pulse, an
input pulse of this duration will significantly enhance the
resolution performance of the Optical Time Domain Reflectometer
presently in operation.

The circuit used in this developmental optical pulser employs a
charged delay line as the energy storage element, with an n-p-n
transistor operating in the avalanche mode as a switch connecting
the delay line to a GaAs laser diode. A series of experiments
were performed, using both RCA SG2000 series laser diodes and the
Laser Diode Laboratories LD-6, series diodes. The choice of the
switching transistor turns out not to be critical, so long as the
reverse collector-to-base breakdown voltage is greater than the
400 to 500 volts needed to charge the delay line. With this
configuration, using a Motorola 2N5550 transistor and microstrip
delay lines of characteristic impedances between 2 and 10 ohms,
15 ns optical pulses of up to 20 watts peak power at 900 nm can
be reliably obtained at rates of 1000 pps.

The experiments described above employed discrete circuit fabri-
cation techniques. Using these techniques, it is possible that
optical pulses as short as 5 ns duration could be generated at
the desired power levels. The limitation on the use of discrete
circuit components results from the effects of distributed induc-
tance throughout the circuit. To obtain a feel for the magnitude
of these effects, at a frequency of 170 MHz, a 1-centimeter
length of conductor has a reactance of about 10 ohms; to produce
20 watt optical pulses using existing GaAs laser diodes, the
driving pulse current approaches 100 amperes. At these current
levels, the inductive voltage drop across even a few millimeters
of conductor becomes substantial as the rise time of the current
driving pulse approaches a few nanoseconds.

The most promising next step appears to be implementation of this
circuit in hybrid form. C. Luddington, of ESED in the Solid
State Sciences Division, fabricated 0.5 ohm resistors on 0.01
ohm-centimeter, single-crystal silicon wafer material and mounted
several of these resistors in headers. Measurements of these
encourage the notion that a hybrid circuit, with the switch
transistor, current-limiting resistor and the laser diode all
mounted in the same header, would greatly reduce distributed
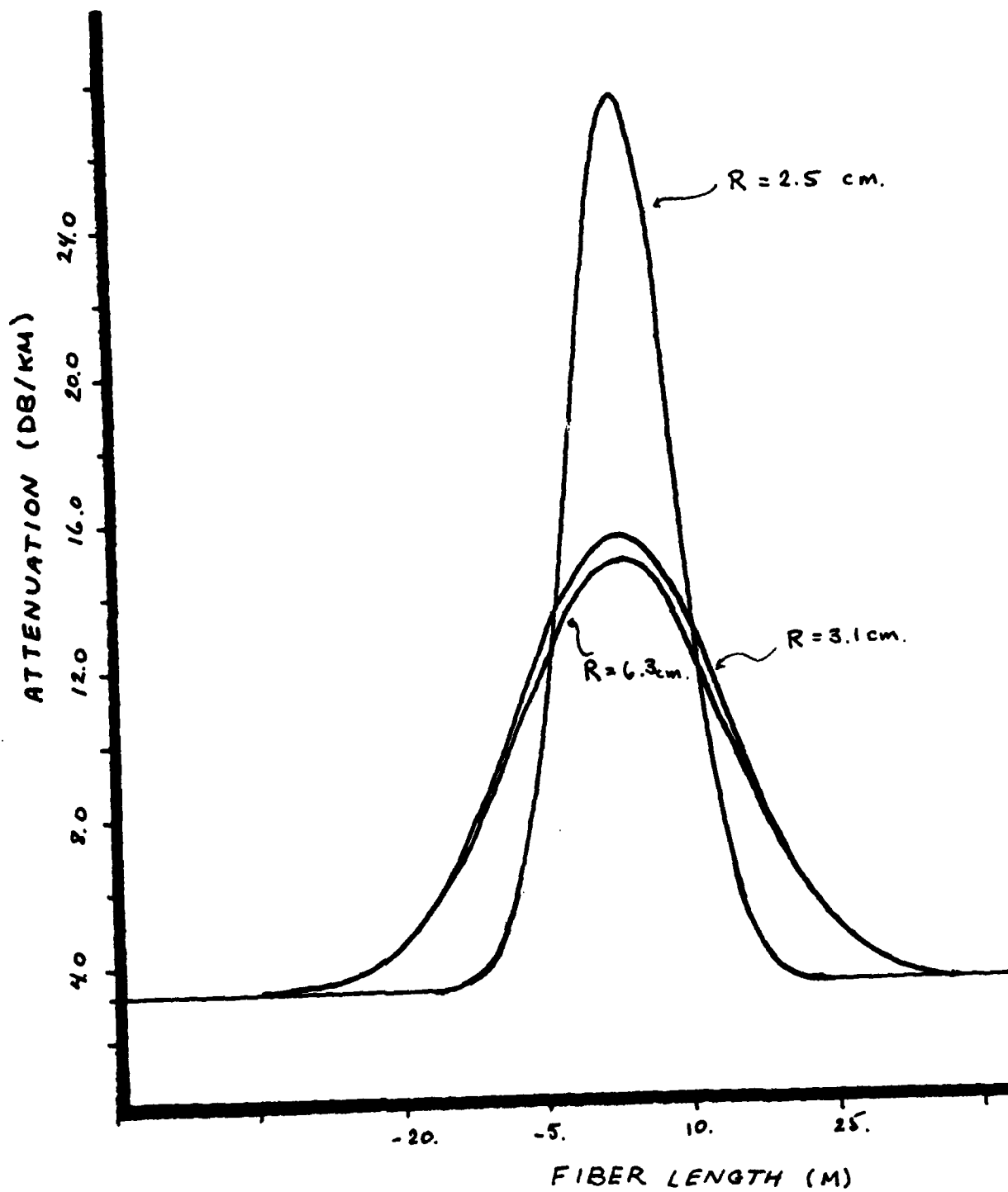inductance in the circuit, hence making possible shorter optical
pulses.

Theory of Optical Time Domain Reflectometry
From Perturbed Fibers

We have developed a theory to describe the Optical Time Domain Reflectometry (OTDR) return signals from weak static perturbations in optical waveguides by employing a time-dependent Green's function formulation. The version of this theory that is applicable to two-dimensional planar waveguides has been presented at the American Ceramic Society's 1980 Chicago meeting and will appear in Advances II: Physics of Fiber Optics. It is included as part of this report[1].

Further calculations for the planar waveguide case have been carried out in order to establish qualitative comparison with experiments that have been performed for perturbations consisting of loops[2] of various diameters ranging from 5 to 12 cm. To facilitate the numerical evaluation of the theory, we have carried out the integration of Equation 37 of Ref.1 analytically. This yields an expression for the backscattered Rayleigh power, that can be written as:

$$\frac{P^{(-)}(t)_{RAYLEIGH}}{P_o} = \alpha_{RAYLEIGH} \cdot \xi \cdot \int_{-\infty}^{\infty} e^{-(t - z' v_g^{-1})^2/\tau^2} .$$

$$\cdot \left\{ \Theta(a - z') \, e^{-2\alpha_{TOT} z'} \right.$$

$$+ (1 - R_i - T_i) \left[\Theta(z' - a) \Theta(a + L - z') e^{-2\alpha_{TOT} z' - 2\alpha_{i RAD}(z' - a)} \right]$$

$$\left. + (1 - R_i - T_i)^2 \Theta(z' - (a+L)) e^{-2\alpha_{TOT} z' - 2\alpha_{i RAD} L} \right\} dz'$$

$$= \alpha_{RAYLEIGH} \cdot \xi \cdot \frac{\sqrt{\pi}}{2} \cdot \tau \, v_g \cdot e^{-t^2/\tau^2} .$$

$$\cdot \left\{ e^{q^2 \tau^2 v_g^2/4} \left[1 + erf(q \tau v_g/2 + a v_g^{-1}/\tau) \right] \right.$$

$$+ e^{2\alpha_{i RAD} \cdot a + q'^2 \tau^2 v_g^2/4} .$$

$$\cdot \left[erf(q' \tau v_g/2 + (a+L) v_g^{-1}/\tau) - erf(q' \tau v_g/2 + a v_g^{-1}/\tau) \right]$$

$$+ e^{-2\alpha_{i RAD} L + q^2 \tau^2 v_g^2/4} .$$

$$\left. \cdot \left[1 - erf(q \tau v_g/2 + (a+L) v_g^{-1}/\tau) \right] \right\}$$

(1)

16

17   figure 1.

where:

$$q = 2(\alpha_{TOT} - t\, v_g^{-1}/\tau^2)$$

$$q' = 2(\alpha_{TOT} - t\, v_g^{-1}/\tau^2 + \alpha_{i\,RAD})$$

In Figure 1. we have plotted the local attenuation in dB/Km vs. the actual position along the waveguide for loops of various diameters for the parameters of the planar model of Ref.1 using the expression for the Rayleigh backscattering power given above in Equation 1.

As mentioned on page 7 of Ref.1, inhomogeneities on a microscopic scale are essentially the mechanism that produces Rayleigh scattering and, for the case of glass fibers, these inhomogeneities are due to thermal fluctuations in density and composition that become frozen in as the glass melt solidifies at temperature Tc. These local fluctuations of density and composition will in turn result in local fluctuations of the refractive index. A calculation of Rayleigh scattering can thus be carried out using the Green's function methods discussed in Ref.1, with the perturbation in refractive index described by

$$\delta n^2(\vec{r}) = \left| \frac{\partial n^2(\vec{r})}{\partial \rho} \right|_{T_c} \Delta \rho(\vec{r}) \tag{2}$$

where $\Delta \rho(\vec{r})$ is the fluctuation in density at point $\vec{r}$.

The scattered field can then be expressed as

$$\delta E_{y\,R_{AY}}^{\mp}(\vec{r},t) = \sum_{n,i} e^{-(t \mp (z_i - z)v_n^{-1} - z_i v_o^{-1})^2/2\tau^2} \left(\frac{\omega_o^2}{2i\,c^2} \right). \tag{3}$$

$$\cdot \frac{u_n(x)}{\beta_n} \left(\frac{-\partial \epsilon}{\partial \rho} \right) \langle o | \Delta \rho_i | n \rangle e^{i\omega_o t \pm i \beta_n z - i(\beta_o \pm \beta_n)z_i}$$

18

where $\langle 0 | \Delta \rho_i | n \rangle$ is the matrix element of the density fluctuation

$$\langle 0 | \Delta \rho_i | n \rangle = \int_{-\infty}^{\infty} u_0(x) \, \Delta \rho(x, z_i) \, u_n(x) \, dx \tag{4}$$

between the incoming mode u_0 and the scattered mode u_n, and i labels the fluctuation volume which is centered around z_i where

$$z_{i+1} - z_i = h$$

The total back-scattered power relative to the input power will be given by (5)

$$\frac{\delta P^{(-)}_{TOT}}{P_0} = \frac{-1}{P_0} \frac{1}{2} \int_{-\infty}^{\infty} \overline{\left(\delta E^{(-)}_{y \, TOT} \frac{i}{\omega \mu_0} \frac{\partial}{\partial z} \delta E^{(-) *}_{y \, TOT} \right)} \, dx$$

where

$$\delta E^{(-)}_{y \, TOT} = \delta E^{(-)}_y + \delta E^{(-)}_{y \, RAY} \tag{6}$$

and the bar indicates a thermal average.

Since

$$\overline{\Delta \rho(z_i)} = 0 \qquad \text{and} \tag{7}$$

$$\overline{\Delta \rho(z_i) \Delta \rho(z_j)} = \delta_{ij} \overline{\Delta \rho^2}$$

the backscattered power from the extrinsic perturbation and the intrinsic frozen in thermal fluctuations will not interfere and the total backscattered power will be simply the sum of the two component powers. The relative backscattered Rayleigh power can be written as

(6)

$$\frac{\delta P^{(-)}_{RAY}}{P_0} = \frac{1}{4} \left(\frac{\omega_0}{c} \right)^4 \sum_{n=0}^{N} \int_{-\infty}^{\infty} e^{-(t - (z' - z) v_n^{-1} - z' v_0^{-1})^2 / \tau^2}$$

$$\times \frac{h}{\beta_0 \beta_n} \left(\frac{\partial \epsilon}{\partial \rho} \right)^2_{T_c} \langle 0 | \Delta \rho(z') n \rangle \langle n | \Delta \rho(z') | 0 \rangle \, dz'$$

19

Instead of pursuing a detailed evaluation of this quantity here, we shall obtain an approximate value for it in a rough way to offer a comparison with the formula derived using ray theory[3]. To do this we first approximate all β_n (and v_n) as being roughly the same and equal to β_o (and v_o). Having made this approximation, we next assume that enough guided modes exist so that the sum over intermediate states can be approximated by the identity operator. The quantity $\overline{\Delta\rho(z)\Delta\rho(z)}$ can then be calculated by thermodynamics[4] to be

$$\overline{\Delta\rho^2} = kT\beta_T \rho^2/V^*$$ (9)

which we further assume to be roughly constant over the guide volume. For purposes of comparison, we take the guide to be planar so that the fluctuation volume can be roughly taken as $V^* \sim ha^2$ with a the guide width. For a multimode step index guide, we approximate $(\beta_o\beta_n)^{-1}$ as

$$\frac{1}{\beta_o^2} \sim \frac{n_1^2 - n_2^2}{n_1^2} \frac{a^2}{(\pi/2)^2}$$ (10)

which then yields a rough upper bound for Rayleigh backscattering in the guide

$$\frac{\delta P^{(-)}_{RAY}}{P_o} \simeq \left(\frac{\omega_o}{c}\right)^4 \left(\rho \frac{\partial\epsilon}{\partial\rho}\right)^2_{T_c} kT\beta_T \frac{(n_1^2 - n_2^2)}{\pi^2 n_1^2}$$ (11)
$$\cdot \int_{-\infty}^{\infty} dz' e^{-(t-(z'-z)v_n^{-1} - z' v_o^{-1})^2/\tau^2}$$

that can be compared with the ray theory formula[3]

$$\frac{\delta P^{(-)}_{RAY}}{P_o} \simeq \left(\frac{\omega_o}{c}\right)^4 \left(\rho \frac{\partial\epsilon}{\partial\rho}\right)^2_{T_c} kT\beta_T \frac{(n_1^2 - n_2^2)}{16\pi n_1^2}$$ (12)
$$\cdot \int_{-\infty}^{\infty} dz' e^{-(t-(z'-z)v_n^{-1} - z' v_o^{-1})^2/\tau^2}$$

The Green's function formulation for OTDR in planar waveguides may be extended to the case of circular fiber guides in a straightforward manner. Replacing the eigenfunctions $u_i(x)$ of the planar guide by $u_{l,n}(\vec{r})$ where l,n designate the angular and radial mode numbers with r the radial coordinate, the Green's function for the circular case may be written as

$$G^{\circ}(\vec{r},\vec{r}';\omega) = \frac{i}{2} \sum_{\hat{n}} \frac{1}{\beta_{\hat{n}}} u_{\hat{n}}^{*}(\vec{r}') u_{\hat{n}}(\vec{r}) e^{-i\beta_{\hat{n}}|3-3'|} \quad (13)$$

where the summation symbol indicates an integral continuum state as well as summation over the bound modes which we abbreviate as $\hat{n} = \{l,n\}$. For an initial pulse with a modal content described by the vector $a_{\hat{n}}$, i.e.,

$$E(\vec{r},t) = \sum_{\hat{n}} a_{\hat{n}} u_{\hat{n}}(\vec{r}) e^{i\omega_{0}t - i\beta_{\hat{n}}3 - (t-t_{0})^{2}/2\tau^{2}} N_{\tau} \quad (14)$$

scattering in the backward or forward direction into the $\hat{k}^{th}$ mode will be given by

$$\delta E_{\hat{k}}^{\mp}(r,t) = \sum_{\hat{n}} e^{i\omega_{0}t - i\beta_{\hat{n}}3} \left(\frac{\omega_{0}^{2}}{2c^{2}}\right) \frac{u_{\hat{k}}(r)}{\beta_{\hat{k}}} a_{\hat{n}} \epsilon_{\hat{n}\hat{k}} \frac{1}{(\beta_{\hat{n}} - \beta_{\hat{k}})} \quad (15)$$

$$\times \left[f_{\hat{n}\hat{k}} e^{-i(\beta_{\hat{n}} - \beta_{\hat{k}})a} - g_{\hat{n}\hat{k}} e^{-i(\beta_{\hat{n}} - \beta_{\hat{k}})(a+L)} \right] N_{\tau}$$

where

$$\epsilon_{\hat{n}\hat{k}} = 2\pi \int_{0}^{\infty} u_{\hat{k}}^{*}(r) \left[\delta n^{2}(r)\right] u_{\hat{n}}(r) r \, dr \quad (16)$$

and where we have assumed an abrupt transition for the perturbed region starting at z = a and extending to z = a+L . For this case

$$f_{\hat{n}\hat{k}} = e^{-\frac{1}{2}(t \mp (a-3)v_{\hat{k}}^{-1} - a v_{\hat{n}}^{-1})^{2}/\tau^{2}} \quad (17a)$$

21

and

$$g_{\hat{n}\hat{\imath}} = e^{-\frac{1}{2}(t \mp (a+L-z)v_{\hat{\imath}}^{-1} - (a+L)v_{\hat{n}})^2/\tau^2} \qquad (17b)$$

The expressions for transition loss and reflected power are essentially the same as those for the planar case with the set $\hat{n} = \{l, n\}$ replacing the transverse mode number n in the planar case. As an example, the expression for the power lost due to transition radiation will be given by

$$\frac{\delta P_{TR}(t)}{P_o} = \frac{k_o^4}{4\sqrt{\beta_{\hat{m}}}} \sum_{\hat{n} \geq \hat{m}} \int d\beta_k \frac{1}{\rho_k} \frac{\epsilon_{\hat{n}\hat{\imath}} \epsilon_{\hat{m}\hat{\imath}}^* a_{\hat{n}} a_{\hat{m}}^*}{(\beta_{\hat{n}} - \beta_{\hat{\imath}})(\beta_{\hat{m}} - \beta_{\hat{\imath}})} \qquad (18)$$

$$\cdot \left\{ \left[2 f_{\hat{n}\hat{\imath}} f_{\hat{m}\hat{\imath}} \cos[(\beta_{\hat{n}} - \beta_{\hat{m}})a] \right. \right.$$

$$+ 2 g_{\hat{n}\hat{\imath}} g_{\hat{m}\hat{\imath}} \cos[(\beta_{\hat{n}} - \beta_{\hat{m}})(a+L)]$$

$$- 2 f_{\hat{n}\hat{\imath}} g_{\hat{m}k} \cos[(\beta_{\hat{n}} - \beta_{\hat{\imath}})a - (\beta_{\hat{m}} - \beta_{\hat{\imath}})(a+L)]$$

$$- 2 f_{\hat{m}\hat{\imath}} g_{\hat{n}k} \cos[(\beta_{\hat{m}} - \beta_{\hat{\imath}})a - (\beta_{\hat{n}} - \beta_{\hat{\imath}})(a+L)] \right]$$

$$\left. \cdot [1 - \delta_{\hat{n}\hat{m}}] +$$

$$\left[f_{\hat{n}\hat{\imath}}^2 + g_{\hat{n}\hat{\imath}}^2 - 2 f_{\hat{n}\hat{\imath}} g_{\hat{n}\hat{\imath}} \cos[L(\beta_{\hat{n}} - \beta_{\hat{\imath}})] \right] \delta_{\hat{n}\hat{m}} \right\}$$

The transverse eigenfunctions for the step index circular guide
are more complex than those for the planar guide, with Bessel
functions replacing simple exponentials[5]. For the case of the
bend perturbation, the double sum in the expressions for
scattered power can be simplified due to the selection rule

$$(19)$$

$$\int_{-\infty}^{\infty} \int_{0}^{2\pi} u_{\ell n}(r) \cos(\ell\varphi) \left[r\cos(\varphi) \right] u_{\ell' m} \cos(\ell'\varphi) \, r \, dr \, d\varphi$$

$$= \frac{\pi}{2} \delta_{\ell \pm \ell' \pm 1} \int_{0}^{\infty} u_{\ell n}(r) \, u_{\ell' m}(r) \, r^2 \, dr$$

which allows transitions only to final states ℓ' that differ from
the initial state ℓ by one unit of the angular mode number.

The radial portion of the transverse matrix element may be
evaluated by reexpressing the integrals involving products of
Bessel functions as

$$(20)$$

$$\int_{0}^{a} J_{\ell+1}(\varkappa r) \, J_{\ell}(\varkappa' r) \, r^2 \, dr$$

$$= \left(\frac{\ell}{\varkappa} - \frac{\partial}{\partial \varkappa} \right) \int_{0}^{a} J_{\ell}(\varkappa r) \, J_{\ell}(\varkappa' r) \, r \, dr$$

$$= \left(\frac{\ell}{\varkappa} - \frac{\partial}{\partial \varkappa} \right) \left\{ \frac{a}{\varkappa^2 - \varkappa'^2} \left[\varkappa \, J_{\ell+1}(\varkappa a) \, J_{\ell}(\varkappa' a) \right. \right.$$

$$\left. \left. - \varkappa' \, J_{\ell}(\varkappa a) \, J_{\ell+1}(\varkappa' a) \right] \right\}$$

with similar expressions for the products of the other Bessel
functions. The complete list of integrals needed for the
calculation of $\epsilon_{\hat{n}\hat{k}}$ for the case of bends is given in Appendix A.

23

The only other remaining difference between the circular and planar calculation for OTDR from bends comes from the expression for radiation loss due to tunneling. For the circular case, this is given by[6]

$$\alpha_{\ell,n\,RAD} = \frac{\sqrt{\pi}\; n_{n}^{2}\; e^{\left[-\frac{2}{3}\left(\gamma_{n}^{3}/\beta_{n}^{2}\right)R\right]}}{e_{\ell}\; V^{2}\; \gamma_{n}^{3/2}\; R^{1/2}\; K_{\ell-1}(\gamma_{n}a)\, K_{\ell+1}(\gamma_{n}a)} \tag{21}$$

which has the same exponential dependence upon the bend radius R as does the two-dimensional case plus an additional factor $R^{1/2}$ in the denominator.

A computer code to evaluate OTDR returns from bends in circular fibers has been prepared and is in the process of being debugged.

REFERENCES

1) Yukon, S.P. and Bendow, B., "Theory of Optical Time Domain Reflectometry from Perturbed Fibers".

2) Rourke, M.D., Private communication, Hughs Research Laboratories.

3) Dakin, J.P. and Gambling, W.A., "Theory of Scattering from the Core of a Multimode Fibre Waveguide", Optics Comm. $\underline{10}$, 195 (1974).

4) Fabelinskii, I.L., "Molecular Scattering of Light", Plenum Press, NY (1968).

5) Marcuse, D., "Theory of Dielectric Optical Waveguides", Academic Press, NY (1974).

6) Marcuse, D., J. Opt. Soc. Am. $\underline{66}$, 216 (1976).

APPENDIX A

The integrals needed to evaluate the transverse matrix element
for the case of bends in a step index fiber are tabulated below:

(A1)
$$\int_0^a r^2 \, J_{\nu+1}(\varkappa r) \, J_\nu(\sigma r) \, dr =$$

$$= \frac{a}{(\varkappa^2 - \sigma^2)} \Big\{ 2\nu \cdot J_{\nu+1}(\varkappa a) \, J_\nu(\sigma a)$$

$$- a \left(\sigma J_{\nu+1}(\varkappa a) \, J_{\nu+1}(\sigma a) + \varkappa J_\nu(\varkappa a) \, J_\nu(\sigma a) \right\}$$

$$+ \frac{2 a \varkappa}{(\varkappa^2 - \sigma^2)^2} \Big\{ \varkappa J_{\nu+1}(\varkappa a) \, J_\nu(\sigma a) - \sigma J_\nu(\varkappa a) \, J_{\nu+1}(\sigma a) \Big\}$$

(A2)
$$\int_a^\infty r^2 \, H^{(1)}_{\nu+1}(i\gamma r) \, H^{()}_\nu(\rho r) \, dr =$$

$$= \frac{a}{(\gamma^2 + \rho^2)} \Big\{ 2\nu \, H^{(1)}_{\nu+1}(i\gamma a) \, H^{()}_\nu(\rho a)$$

$$- i\gamma a \, H^{(1)}_\nu(i\gamma a) \, H^{()}_\nu(\rho a)$$

$$- \rho a \, H^{(1)}_{\nu+1}(i\gamma a) \, H^{()}_{\nu+1}(\rho a) \Big\}$$

$$+ \frac{a}{(\gamma^2 + \rho^2)^2} \Big\{ \gamma H^{(1)}_{\nu+1}(i\gamma a) \, H^{()}_\nu(\rho a)$$

$$+ i \rho \, H^{(1)}_\nu(i\gamma a) \, H^{()}_{\nu+1}(\rho a) \Big\}$$

(A3)
$$\int_0^a r^2 J_\nu(\varkappa r) J_{\nu-1}(\sigma r)\,dr =$$

$$= \frac{a}{(\varkappa^2-\sigma^2)}\Big\{ 2(\nu-1) J_\nu(\varkappa a) J_{\nu-1}(\sigma a) - a\varkappa J_{\nu-1}(\varkappa a) J_{\nu-1}(\sigma a)$$

$$- a\sigma J_\nu(\varkappa a) J_\nu(\sigma a) \Big\}$$

$$+ \frac{2a\varkappa}{(\varkappa^2-\sigma^2)^2}\Big\{ \varkappa J_\nu(\varkappa a) J_{\nu-1}(\sigma a) - \sigma J_{\nu-1}(\varkappa a) J_\nu(\sigma a) \Big\}$$

(A4)
$$\int_a^\infty r^2 H_\nu^{(1)}(i\gamma r) H_{\nu-1}^{()}(\rho r)\,dr =$$

$$= \frac{a}{(\gamma^2+\rho^2)}\Big\{ 2(\nu-1) H_\nu^{(1)}(i\gamma a) H_{\nu-1}^{()}(\rho a)$$

$$- i\gamma a\, H_{\nu-1}^{(1)}(i\gamma a) H_{\nu-1}^{()}(\rho a)$$

$$- \rho a\, H_\nu^{(1)}(i\gamma a) H_\nu^{()}(\rho a) \Big\}$$

$$+ \frac{2a\gamma}{(\gamma^2+\rho^2)^2}\Big\{ \gamma H_\nu^{(1)}(i\gamma a) H_{\nu-1}^{()}(\rho a)$$

$$+ i\rho\, H_{\nu-1}^{(1)}(i\gamma a) H_\nu^{()}(\rho a) \Big\}$$

Using these results, the transverse matrix element for bound to continuum transitions may be expressed (writing $\varkappa$ for $\varkappa_{\nu,i}$ and γ_ν for $\gamma_{\nu,i}$) as

27

$$\text{(A5)} \quad \int_0^\infty u_{\nu+1}(x_{\nu+1}r)\, u_\nu(kr)\, r^2\, dr =$$

$$= A_{\nu+1} B_\nu \left\{ \int_0^a J_{\nu+1}(x_{\nu+1}r)\, J_\nu(\sigma r)\, r^2\, dr \right.$$

$$+ \int_a^\infty \frac{J_{\nu+1}(x_{\nu+1}a)}{H_{\nu+1}^{(1)}(i\gamma_{\nu+1}a)}\, H_{\nu+1}^{(1)}(i\gamma_{\nu+1}r)\left[C H_\nu^{(1)}(\rho r) \right.$$

$$\left. \left. + CD\, H_\nu^{(2)}(\rho r) \right] r^2\, dr \right\}$$

$$= \left[\frac{4(\mu_0/\epsilon_0)^{1/2} \gamma_{\nu+1}^2\, P}{e_{\nu+1}\, \pi a^2 n (n_1^2 - n_2^2) k_0^2} \, \frac{1}{|J_\nu(x_{\nu+1}a)\, J_{\nu+2}(x_{\nu+1}a)|} \right]^{1/2}$$

$$\cdot \left[\frac{(\mu_0/\epsilon_0)^{1/4} (8\rho P)^{1/2}}{(e_\nu n)^{1/2}\, a\, \pi^{3/2} |\sigma J_{\nu-1}(\sigma a) H_\nu^{(1)}(\rho a) - \rho J_\nu(\sigma a) H_{\nu-1}^{(1)}(\rho a)|} \right]$$

$$\cdot \left\{ \frac{a}{(x_{\nu+1}^2 - \sigma^2)}\left[2\nu J_{\nu+1}(x_{\nu+1}a)\, J_\nu(\sigma a) \right. \right.$$

$$\left. - a\left(\sigma J_{\nu+1}(x_{\nu+1}a)\, J_{\nu+1}(\sigma a) + x_{\nu+1} J_\nu(x_{\nu+1}a)\, J_\nu(\sigma a) \right) \right]$$

$$\frac{+2a\, x_{\nu+1}}{(x_{\nu+1}^2 - \sigma^2)^2}\left[x_{\nu+1} J_{\nu+1}(x_{\nu+1}a)\, J_\nu(\sigma a) - \sigma J_\nu(x_{\nu+1}a)\, J_{\nu+1}(\sigma a) \right]$$

$$+ \frac{a J_{\nu+1}(x_{\nu+1}a)}{K_{\nu+1}(\gamma_{\nu+1}a)(\gamma_{\nu+1}^2 + \rho^2)^2}\left[(\gamma_{\nu+1}^2 + \rho^2)\left(\sigma a J_{\nu-1}(\sigma a)\, K_{\nu+1}(\gamma_{\nu+1}a) \right. \right.$$

$$\left. + \gamma_{\nu+1} a J_\nu(\sigma a)\, K_\nu(\gamma_{\nu+1}a) \right)$$

$$+ 2 \gamma_{\nu+1}^2\, J_\nu(\sigma a)\, K_{\nu+1}(\gamma_{\nu+1}a)$$

$$\left. \left. - 2 \gamma_{\nu+1}\, \sigma\, J_{\nu+1}(\sigma a)\, K_\nu(\gamma_{\nu+1}a) \right] \right\}$$

(A6) $\displaystyle\int_0^\infty \mathcal{U}_{\nu-1}(x_{\nu-1}\, r)\, \mathcal{U}_\nu(kr)\, r^2\, dr =$

$$= A_{\nu-1}\, B_\nu \left\{ \int_0^a J_{\nu-1}(x_{\nu-1}r)\, J_\nu(\sigma r)\, r^2\, dr \right.$$

$$\left. + \int_a^\infty \frac{J_{\nu-1}(x_{\nu-1}a)}{H_{\nu-1}^{(1)}(i\gamma_{\nu-1}a)}\, H_{\nu-1}^{(1)}(i\gamma_{\nu-1}r)\left[C\, H_\nu^{(1)}(\rho r) + CD\, H_\nu^{(2)}(\rho r)\right] r^2\, dr \right\}$$

$$= \left[\frac{4\,(\mu_0/\epsilon_0)^{1/2}\,\gamma_{\nu-1}^2\, P}{e_{\nu-1}\,\pi a^2 n\,(n_1^2 - n_2^2)\, k_0^2\, |\, J_{\nu-2}(x_{\nu-1}a)\, J_\nu(x_{\nu-1}a)\,|} \right]^{1/2}$$

$$\times \left[\frac{(\mu_0/\epsilon_0)^{1/4}\,(8\rho P)^{1/2}}{(e_\nu n)^{1/2}\, a\pi^{3/2}\,|\,\sigma J_{\nu-1}(\sigma a)\, H_\nu^{(1)}(\rho a) - \rho J_\nu(\sigma a)\, H_{\nu-1}^{(1)}(\rho a)|} \right]$$

$$\times \left\{ \frac{-a}{(x_{\nu-1}^2 - \sigma^2)}\left[2(\nu-1)\, J_{\nu-1}(x_{\nu-1}a)\, J_\nu(\sigma a) \right.\right.$$

$$\left. - a\left(x_{\nu-1}\, J_\nu(x_{\nu-1}a)\, J_\nu(\sigma a) + \sigma J_{\nu-1}(x_{\nu-1}a)\, J_{\nu-1}(\sigma a) \right)\right]$$

$$+ \frac{2a\sigma}{(x_{\nu-1}^2 - \sigma^2)^2}\left[\sigma J_{\nu-1}(x_{\nu-1}a)\, J_\nu(\sigma a) - x_{\nu-1}\, J_\nu(x_{\nu-1}a)\, J_\nu(\sigma a) \right]$$

$$+ \frac{a J_{\nu-1}(x_{\nu-1}a)}{K_{\nu-1}(\gamma_{\nu-1}a)(\gamma_{\nu-1}^2 + \rho^2)^2}\left[(\gamma_{\nu-1}^2 + \rho^2)\Big(\big(2 J_\nu(\sigma a) - \sigma a\, J_{\nu+1}(\sigma a) \big) \cdot \right.$$

$$\left. \times\, K_{\nu-1}(\gamma_{\nu-1}a) + \gamma_{\nu-1}a\, K_\nu(\gamma_{\nu-1}a)\, J_\nu(\sigma a) \Big) \right.$$

$$\left.\left. - 2\rho^2 K_{\nu-1}(\gamma_{\nu-1}a)\, J_\nu(\sigma a) + 2\gamma_{\nu-1}\sigma\, J_{\nu-1}(\sigma a)\, K_\nu(\gamma_{\nu-1}a) \right] \right\}$$

29

ATTACHMENT A

FRESNEL ZONE PLATES FOR WAVELENGTH DEMULTIPLEXING

by

Haim M. Haskal*

Parke Mathematical Laboratories

Carlisle, MA. 01741

An analysis is presented on the application of Fresnel zone plates to wavelength demultiplexing in fiber optic systems. A demultiplexer consisting of an off-axis Fresnel zone plate acts as a focusing spectrometer. Blazed Fresnel zone plates have high efficiency over a 20% bandwidth and can demultiplex a large number of channels.

30

INTRODUCTION

Present day optical fibers have capacities which exceed by far the bandwidths required to transmit high speed modulated light signals. To increase the bandwidth utilization of the fiber several light carriers can be simultaneously transmitted - multiplexed - over the same fiber and separated by wavelength - demultiplexed - at the receiving end. The first proponent of wavelength multiplexing was Tomlinson at Bell Telephone Laboratories who analyzed [1] in detail the requirements and techniques for optical multiplexing. Optical demultiplexers based on blazed diffraction gratings were demonstrated by Tomlinson,[2],[3] and Aoyama[4]. Other types of demultiplexers based on interference filters[5], prisms[6], and aberration corrected concave gratings[7] were also demonstrated.

In this paper we analyze the performance of a wavelength demultiplexer based on a Fresnel zone plate. The zone plate performs simultaneously the functions of wavelength dispersion and focusing.

FRESNEL ZONE PLATE THEORY

Fresnel zone plates (FZP) have been used as lenses and as spectrometers in various regions of the electromagnetic spectrum. An excellent article reviewing the properties of FZP was published by Young[8]. The usual type FZP consists of a series of alternating opaque and transparent annular zones. This FZP is characterized by a transmission function (for an infinite plate)

$$t(r) = \frac{1}{2} + \frac{1}{2} \, \text{sgn} \left(\cos \frac{kr^2}{2f} \right) \tag{1}$$

where r is the radial coordinate in the FZP plane, $k = 2\pi/\lambda$, λ is the wavelength, f the focal length.

For a normally incident unit plane wave the transmitted electric field can be expanded in a Fourier series

$$E(z,r) = \exp(-jkz) \sum_{n=-\infty}^{\infty} \frac{\sin \frac{n\pi}{2}}{n\pi} \, \exp\left(j \frac{nkr^2}{2f}\right) \tag{2}$$

In Eq. (2) the terms with n negative represent spherical waves converging toward real foci of coordinates$(0, \frac{f}{|n|})$. Similarly the terms with n positive represents spherical waves diverging from virtual foci located at coordinates $(0, \frac{-f}{|n|})$ as shown in Fig. 1. The fraction of the incident light diverted to the first real focus is called the efficiency of the FZP and in this case is given by

$$\eta = \frac{1}{\pi^2} \approx 10\%.$$

A more efficient zone plate can be constructed by replacing the opaque zones, which obstruct 50% of the incident light, by transparent zones which introduce a half wave retardation between adjacent zones as shown in Fig. 2. Such a zone plate is called a phase reversal zone plate and is also characterized by multiple foci but has an efficiency η given by

$$\eta = \frac{4}{\pi^2} \approx 40\%.$$

The focal length f for both types of Fresnel zone plates mentioned above can be related to the zone number m and the radius of the mth zone by

$$f = \frac{r_m^2}{m\lambda} \tag{3}$$

Let the focal length of the FZP be f_0 at a wavelength λ_0 then at an arbitrary wavelength λ we have

$$f(\lambda) = f_0 \frac{\lambda_0}{\lambda} \tag{4}$$

Equation (4) puts in evidence the high dispersion of FZP's which can be used advantageosuly in wavelength demultiplexing.

To improve the efficiency of the FZP beyond the 40% that is possible with the phase reversal zone plate one can use the phase Fresnel lens concept introduced by Miyamoto[9] in 1961. Instead of introducing an abrupt phase retardation of $\lambda/2$ at the edge of a zone as in the phase reversal zone plate, in Miyamoto's phase Fresnel lens one introduces a gradual phase retardation over a zone, according to some profile, from zero to a maximum of λ. The

32

adjacent zone starts again from a zero phase retardation which is indistinguishable from the λ retardation at the edge of the previous zone. In this way the phase retardation appears continuous for the incident light even though the actual phase plate has a dentelated profile. The procedure of constructing a phase Fresnel lens corresponding to a plano-convex lens is illustrated in Fig. 3.

The phase Fresnel lens, also referred to as the blazed Fresnel zone plate (BFZP), as designed in Fig. 3 will focus a plane wavefront at the design wavelength λ_0 to a single focus just like the original lens. However, if the wavelength is changed from λ_0 to λ some of the light is focused to higher order foci. We will now examine the effect of changing the wavelength on the efficiency of the BFZP.

Let the BFZP introduce a quadratic wavefront deformation given by the phase function

$$\phi(u,v) = -(u^2+v^2)/2f_0 \tag{5}$$

where u and v are transverse coordinates in the plane of the plate and f_0 its focal length at the wavelength λ_0.

The phase transformation, similar to that produced by a thin lens, is characterized by a transmission function (over each zone)

$$t(u,v) = \exp\left[-j\frac{k}{2f_0}(u^2+v^2)\right] \tag{6}$$

The focal length of the BFZP obeys the relation given by Eq. (4). At an arbitrary wavelength the transmission function can be expanded (over each zone) as

$$\exp(-j2\pi\phi/\lambda) = \sum_{\ell=-\infty}^{\infty} A_\ell \exp(-j2\pi\ell\phi/\lambda) \tag{7}$$

where

$$\phi(u,v) = \frac{\lambda}{\lambda_0}\phi(u,v)$$

33

Substituting for the coefficients A_ℓ in eq. (7) we obtain

$$\exp(-j2\pi\phi/\lambda) = \frac{\sin \pi(\lambda_0-\lambda)/\lambda}{\pi(\lambda_0-\lambda)/\lambda} \exp\{-j2\pi\theta/\lambda-j\pi(\lambda_0-\lambda)/\lambda\}$$

$$\times \left[1 + \frac{\lambda_0-\lambda}{\lambda_0}\exp(j2\pi\theta/\lambda) + \frac{\lambda_0-\lambda}{\lambda_0-2\lambda}\exp(-j2\pi\theta/\lambda)+\dots\right]. \tag{8}$$

At the design wavelength λ_0 only the first term in the series survives corresponding to a single real focus. As one deviates from λ_0 higher order foci appear. To estimate the fraction of energy diffracted at the first real focus, i.e. the efficiency η, as a function of wavelength, we consider the coefficient of the first term in Eq. (8). The efficiency is given by

$$\eta = \left[\frac{\sin \frac{\pi\Delta\lambda}{\lambda_0}(1 + \frac{\Delta\lambda}{\lambda_0})}{\frac{\pi\Delta\lambda}{\lambda_0}(1 + \frac{\Delta\lambda}{\lambda_0})}\right]^2 \tag{9}$$

where $\Delta\lambda$ is the deviation from the design wavelength λ_0. If we set $\Delta\lambda/\lambda_0 = \pm 10\%$ in Eq. (9) we obtain the value 0.96; thus only 4% of the energy is diffracted into the zero and higher order foci. A BFZP can therefore be an efficient demultiplexer with 20% bandwidth. Such a bandwidth can accommodate 10 optical channels 20 nm apart around a center wavelength $\lambda_0 = 1.0$ μm.

THE USE OF THE BFZP FOR WAVELENGTH DEMULTIPLEXING

The BFZP can be used in several configurations (reflection, transmission) as a dispersive and focusing device for wavelength demultiplexing. It has, in fact, been proposed for use as a focusing spectrometer at soft x-ray wavelengths[10]. One cannot use a full BFZP for demultiplexing because the images of the input fiber at the various wavelengths appear along the axis one in the shadow of the other. If an array of detectors is placed at the image positions, the first detector will obstruct some of the light meant to reach the others, in addition crosstalk between channels will be very high. To alleviate this problem one can use an off-axis BFZP; light is now focused towards the various images only from one side of the plate and the array of channel detectors can be placed along the BFZP axis or at an angle to the axis without interference.

We illustrate the use of a BFZP in an off-axis configuration in Fig. 4. The light emanating from a multimode optical fiber is collimated prior to entering the BFZP. Two adjacent optical channels at λ_0 and $\lambda_0 + \Delta\lambda$ are focused at F_1 and F_2. The separation between the two channels along the axis can be obtained from Eq. 4 and is given by

$$\Delta f = f \frac{|\Delta\lambda|}{\lambda_0} \tag{10}$$

where $\Delta\lambda$ is the wavelength separation between the channels. From Eq. (10) one determines the size of photodetectors as a function of the BFZP focal length and wavelength. The light impinges on the detectors located along the axis at a very shallow angle, close to grazing incidence and therefore the reflection loss can be considerable. It is, therefore, necessary to coat the photodetectors with antireflection coating suitable for that angle of incidence.

We have shown in Fig. 5 a two-channel demultiplexer with the detectors inclined at an angle δ to the BFZP axis; they are located such as to intercept all the light from the respective image of the fiber.

35

The angle δ is determined from the geometry

$$\tan \delta = \frac{r_m - D + \epsilon a}{f} \tag{11}$$

where r_m is the radius of the mth zone of the BFZP, $\underline{D}$ is the diameter of the collimated beam, $\underline{\epsilon}$ is the angle of divergence of the collimated beam, $\underline{a}$ is the distance between the collimating lens and the BFZP.

We also have the following relations

$$D = 2(NA) f_{col} \tag{12}$$

where (NA) is the numerical aperture of the fiber, $\underline{f_{col}}$ the focal length of the collimating lens.

$$\epsilon = \frac{f}{f_{col}} \, d_{core} \tag{13}$$

where d_{core} is the core diameter of the fiber.

From Eq.(3) we obtain the relation

$$\frac{f}{r_m} = \frac{\Delta r}{\lambda} \tag{14}$$

where $\underline{r}$ is the width of the $\underline{m}^{th}$ zone. Substituting into Eq. (11) we obtain

$$\tan \delta = \frac{\lambda}{\Delta r} - 2(NA) \frac{f_{col}}{f} \tag{15}$$

36

where we have assumed that the term εa in Eq.(11)is negligible.
If one uses a unity magnification imaging system $\frac{f_{col}}{f} = 1$; NA = 0.2, λ = 1 μm
and Δr = 1 μm we obtain

$$\tan \delta = 0.6 \quad \therefore \quad \delta = 30.96^{\circ}$$

Thus in this case the antireflection coating for the photodetector must be
designed for light incident at 59° with respect to the normal if the detector is
placed along the axis of the BFZP. If the detectors are inclined at angle
δ with respect to the axis the antireflection coating should be designed
for an incidence angle of 28° with respect to the normal to the photodetector.

The dimensions of the BFZP need not be very large and are compatible with
fiber optic systems. If we choose f = f_{col} = 6 mm ,λ = 1 μm , Δr = 1 μm, the
diameter of the collimated beam equal to the off-axis BFZP diameter is

$$D = 2 \ (NA)f_{col} = 2.4 \ mm$$

The number of zones which must be ruled is readily computed to be 1920.

FABRICATION CONSIDERATIONS

To fabricate a blazed Fresnel zone plate several avenues are open:

a) Diamond point turning. Considerable progress has been reported in the
last few years in the design and implementation of computer controlled diamond
turning machines. Such machines are capable of generating the required phase
profile in soft plastic materials to produce a BFZP.

b) Computer generated phase profiles. It has been shown about a decade ago that
a computer generated phase hologram, labelled a kinoform, is entirely equivalent
to a phase Fresnel lens. A good bibliography on this subject is found in
Clair and Abitbol[11].

c) <u>Holographic generation.</u> Instead of producing a relief pattern one can induce a change in the refractive index of certain materials by exposure to light and realize a Fresnel zone plate. Opterating near the Bragg angle such a Fresnel plate has high dispersion and focusing power just like the BFZP. Recent advances in the fabrication of dichromated gelatin have resulted in very large index changes in the material under exposure to light. This makes dichromated gelatin an attractive material for infrared applications. Some problems still remain to be solved because the material must be exposed with visible light (for maximum sensitivity) and used with infrared light for fiber optic systems. Such a wavelength shift between construction and r..con-struction introduces severe aberrations.

CONCLUSIONS

An off-axis BFZP constitutes an attractive candidate for a multichannel near infrared fiber optic demultiplexer. More research must be devoted to devise methods of producing a BFZP.

REFERENCES

1. W.J. Tomlinson "Wavelength Multiplexing in Multimode Optical Fibers" Appl. Opt. 16, pp 2180-2194 (1977).

2. W.J. Tomlinson and G.D. Aumiller "Optical Multiplexer for Multimode Fiber Transmission Systems" Appl. Phys. Lett. 31, pp 169-171 (1977).

3. W.J. Tomlinson and C. Lin "Optical Wavelength - Division Multiplexer for the 1-1.4 μm Spectral Region" Electron Lett. 14, pp 345-347 (1978).

4. K. Aoyama and J. Minowa "Low-Loss Optical Demultiplexer for WDM Systems in the 0.8-μm Wavelength Region" Appl. Opt. 18, pp 2834-2836 (1979).

5. K. Nosu, H. Ishio and K. Hashimoto "Multireflection Optical Multi/ Demultiplexer Using Interference Filters" Electron. Lett. 15, pp. 414-415 (1979).

6. S. Sugimoto, K. Minemura, K. Kobayashi, M. Seki, M. Shikada, A. Ueki and T. Yanase "High-Speed Digital Signal Transmission Experiments by Optical Wavelength-Division Multiplexing" Electron. Lett. 13, pp 680-682 (1977).

7. R. Watanabe, K. Nosu, T. Harada and T. Kita: "Optical Demultiplexer Using Concave Gratings in the 0.7-0.9 μm Wavelength Region", Electron. Lett. 16, pp. 106-108 (1980).

8. M. Young "Zone Plates and Their Aberrations", J. Opt. Soc. Am. 62, pp. 972-976 (1972).

9. K. Miyamoto "The Phase Fresnel Lens" J. Opt. Soc. Am. <u>51</u>, pp 17-20 (1961).

10. N.M. Ceglio, D.C. Shavers, D.C. Flanders and H.I. Smith "Micro-Fresnel
    Structures for Microscopy of Laser Generated Bright X-ray Sources" presented
    at New York Academy of Sciences Conference on Ultrasoft X-ray Microscopy,
    June 13-15, 1979, New York, N.Y.

11. J. J. Clair and C.I. Abitbol "Recent Advances in Phase Profile
    Generation" in Progress in Optics Vol. XVI, ed. (North Holland
    Publishing Company, 1978).
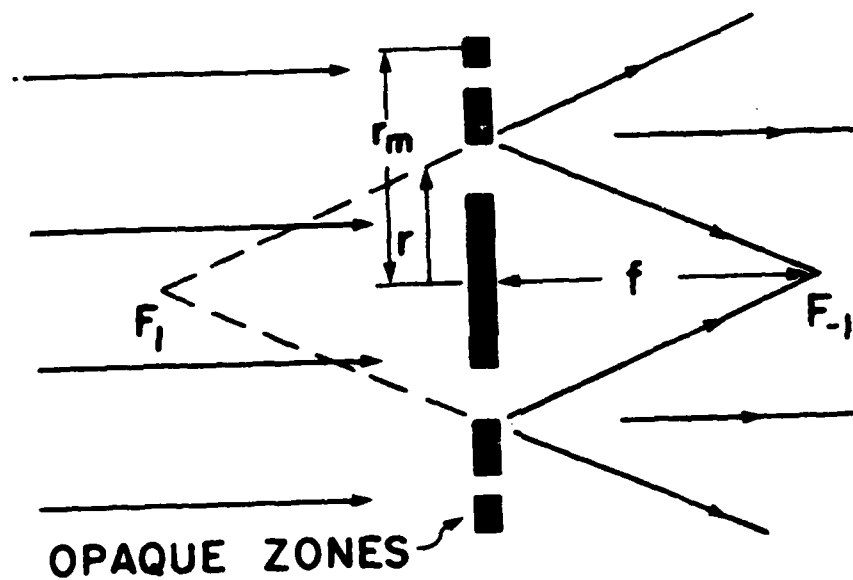
Fig. 1   Fresnel zone plate
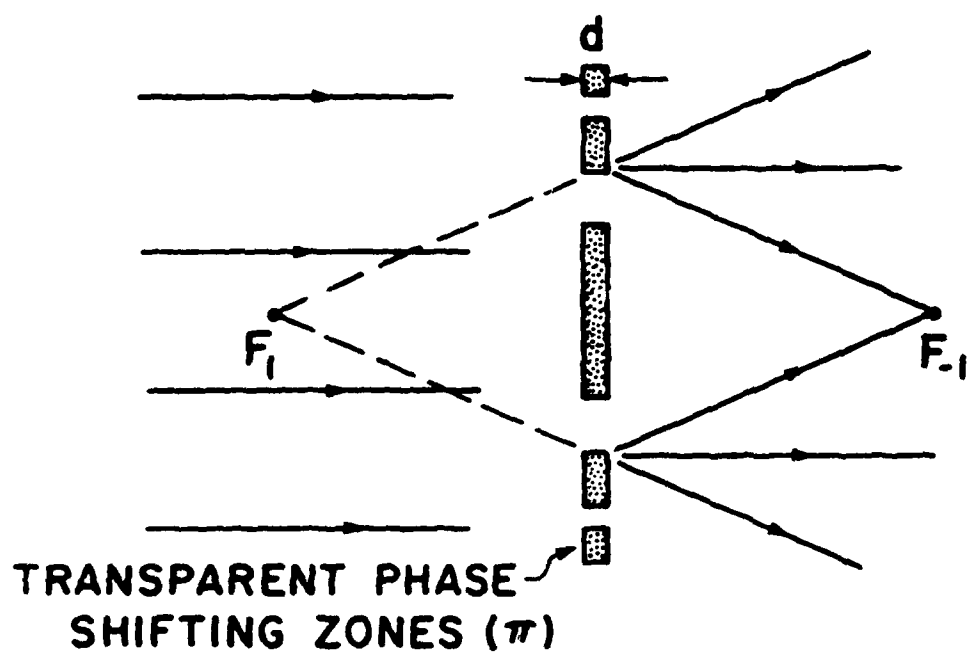
Fig. 2   Phase reversal Fresnel zone plate $d = \frac{\lambda}{2(n-1)}$, n is the
          refractive index.
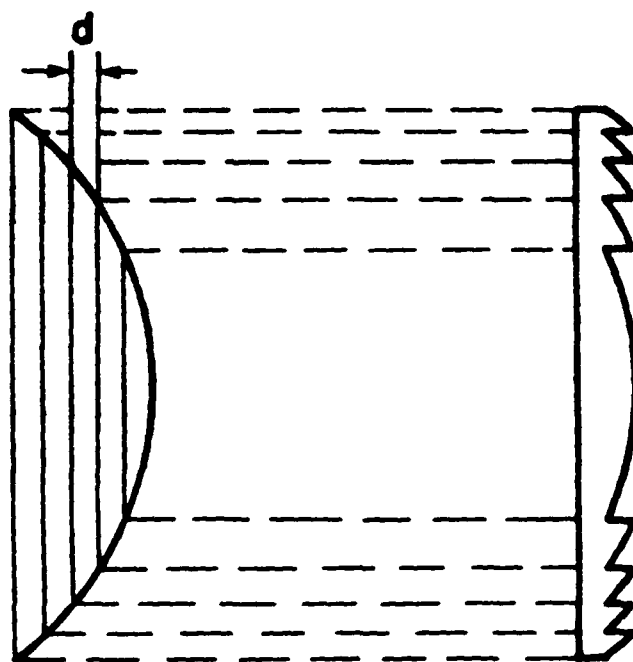
Fig. 3   Blazed Fresnel zone plate construction equivalent to spherical
lens $d = \frac{\lambda}{n-1}$

BFZP

MULTIMODE
FIBER

COLLIMATOR

λ_2

λ_1

F_1 F_2
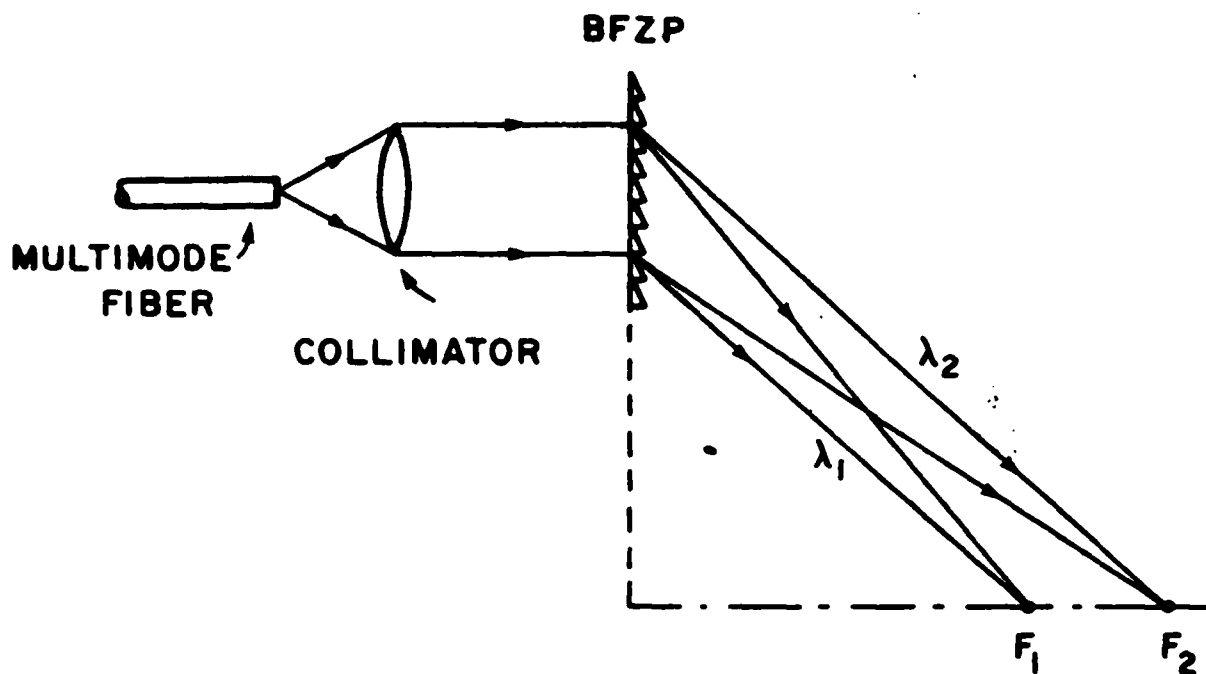
Fig. 4   Off-axis BFZP demultiplexer.

44
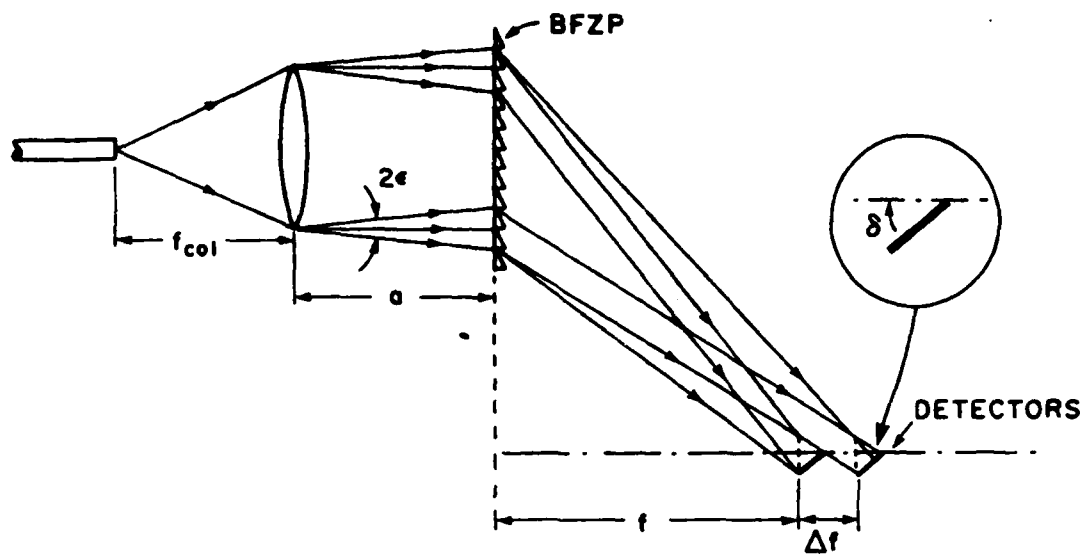
Fig. 5   2-channel BFZP demultiplexer with detectors.

45

ATTACHMENT B

THEORY OF OPTICAL TIME DOMAIN REFLECTOMETRY

FROM PERTURBED FIBERS

Stanford P. Yukon*
Parke Mathematical Laboratories
Carlisle, Massachusetts 01741

Bernard Bendow
Solid State Sciences Division, Rome Air Development Center
Hanscom AFB, Massachusetts 01731

ABSTRACT

We formulate a theory of backscattering from static perturbations in fibers, and apply the results to predict the OTDR signal for perturbations such as bends. A variety of effects are examined in detail, such as transition loss, curvature loss, dependence on mode number and dependence on pulsewidth.

I. INTRODUCTION

In optical time-domain reflectometry (OTDR), optical pulses are launched into a fiber waveguide and the back-scattered signal is measured as a function of time [1]. For a uniform unperturbed fiber the OTDR signal consists entirely of Rayleigh back-scattering, and displays an exponential decrease as a function of time due to the absorptive and scattering losses of the fiber. In this work we examine backscattering from static perturbations (slowly varying compared to the pulse width) in optical waveguides. The exponentially decreasing OTDR intensity will in this case be modified due to reflections and radiation losses induced by the perturbation. Corresponding changes will also occur of course in the spatial and temporal makeup of the pulse although we do not consider these here.

In order to calculate the OTDR return, we employ a time-dependent Green's function (GF) method. Although the equations derived in this way are intractable in general, it is possible to obtain explicit but approximate expressions for the case of weakly perturbed fibers by approximating the exact GF's by their unperturbed counterparts. One fortunate consequence of the lowest order theory is that the contributions to the OTDR intensity from random scattering processes (i.e., Rayleigh scattering) and from deterministic perturbations do not interfere.

The detailed properties of the backscattered signal depend, of course, on the specific form of the perturbation and the characteristics of the waveguide. Nevertheless, certain general features emerge from the present formulation as illustrated by the specific example of bend perturbations. For example, when a uniformly perturbed region is involved, then the net scattering from the interior of the perturbed region vanishes, leaving contributions from just the ends. In higher order, modes may mix in the interior and tunnel cut of the guide as well. In general both reflections and transition losses will be manifested in the OTDR signal, with the characteristics of this signal depending on the symmetry of the perturbation. For example, for a single mode waveguide reflection will be totally absent in lowest order if the perturbation possesses odd symmetry, but is present for even symmetry. Transition losses, on the other hand, will occur in either instance. We perform a variety of computations to illustrate the dependence of OTDR from bends on launch

47

conditions, pulsewidth, bend length, and bend radius.

II. GREEN'S FUNCTION THEORY FOR PROPAGATION IN PERTURBED WAVEGUIDES

In this section we utilize time-dependent GF theory to obtain an
expression for the change in the time-dependent field amplitude in a fiber
induced by a perturbation. The results will be used in subsequent sections
to evaluate the OTDR return from fiber bends.

For the case of fiber waveguides for which the difference between
core and cladding refractive indices is small, which includes the majority
of waveguides of interest, the vector wave equation for the waveguide modes
may be approximated by equivalent scalar equations for TE and TM modes. Taking
z as the propagation direction and assuming solutions of the form

$$\vec{E}(x,y,z,t) = \vec{E}(x,y)\, e^{i\omega t - i\beta z}, \tag{1}$$

the wave equation for TE modes may be written as

$$\left\{ \frac{\partial^2}{\partial x^2} + \frac{\partial^2}{\partial y^2} + \left(\frac{\omega^2}{c^2} n^2(x,y,z) - \beta^2 \right) \right\} E_y(x,y) = 0. \tag{2}$$

For simplicity we first consider the case of planar waveguides. In this
instance we have

$$n^2(\vec{r}) = n^2(x,z) = n_0^2(x) + \delta n^2(x,z) \tag{3}$$

where $n_0^2(x)$ represents the unperturbed guide and $\delta n^2(x,z)$ the perturbation.

Eigensolutions for the unperturbed guide

$$\left\{ \frac{\partial^2}{\partial x^2} + \left(\frac{\omega^2}{c^2} n_0^2(x) - \beta_n^2 \right) \right\} u_n(x) = 0 \tag{4}$$

can be used to construct the GF for the unperturbed guide as [2]

$$G^0(\vec{r},\vec{r}';\omega) = \frac{1}{2\pi} \sum_n \int \frac{u_n^*(x')u_n(x)e^{-i\Lambda(z-z')}}{\beta_n^2 - \Lambda^2} \, d\Lambda$$

$$+ \frac{1}{2\pi} \int d\beta_k \int \frac{u_k^*(x')u_k(x)e^{-i\Lambda(z-z')}}{\beta_k^2 - \Lambda^2} \, d\Lambda \tag{5}$$

which can, by contour integration, be reduced to

$$G^0(\vec{r},\vec{r}';\omega) = \frac{i}{2} \sum_n \frac{1}{\beta_n} u_n^*(x')u_n(x)e^{-i\beta_n|z-z'|} \tag{6}$$

where the summation symbol will now be used to indicate an integral over all continuum states as well as summation over bound waveguide modes. By construction $G^0(\vec{r}, \vec{r}';\omega)$ satisfies the differential equation

$$\left\{ \left(\frac{\partial^2}{\partial x^2} + \frac{\omega^2}{c^2} n_0^2(x) \right) + \frac{\partial^2}{\partial z^2} \right\} G^0(\vec{r}, \vec{r}';\omega) = \delta(x-x') \, \delta(z-z') \tag{7}$$

The full GF $G(\vec{r}, \vec{r}';\omega)$ that satisfies

$$\left\{ \left(\frac{\partial^2}{\partial x^2} + \frac{\partial^2}{\partial z^2} + \frac{\omega^2}{c^2} n_0^2(x) \right) + \frac{\omega^2}{c^2} \, \delta n^2(x,z) \right\} G(\vec{r}, \vec{r}';\omega) = \delta(x-x') \, \delta(z-z') \tag{8}$$

may then be determined by iteration, with the initial approximation to $G(\vec{r}, \vec{r}';\omega)$ being given by $G^0(\vec{r}, \vec{r}';\omega)$; thus

$$G(\vec{r},\vec{r}';\omega) = G^0(\vec{r},\vec{r}';\omega) + \int G^0(\vec{r}\,\vec{r}'';\omega) \frac{\omega^2}{c^2} \delta n^2(\vec{r}'') \, G^0(\vec{r}''\,\vec{r}')d\vec{r}'' \tag{9}$$

$$+ \int\int G^0(\vec{r}\vec{r}'') \frac{\omega^2}{c^2} \delta n^2(\vec{r}'')G^0(\vec{r}''\,\vec{r}''') \frac{\omega^2}{c^2}\delta n^2(\vec{r}''')G(\vec{r}'''\vec{r}')d\vec{r}''\,d\vec{r}''' + \ldots$$

The scattered wave produced by the perturbed waveguide in response to an incident wave E^0 can then be expressed using the full GF as

49

$$\delta E_y(\vec{r},\omega) = - \int G(\vec{r}\ \vec{r}';\omega)\ \frac{\omega^2}{c^2}\ \delta n^2(\vec{r}')\ E_y^0(\vec{r}')\ d\vec{r}'\ . \tag{10}$$

In order to exhibit a calculation of an OTDR backscattered return using the GF approach in the simplest manner, we shall limit the present calculation to planar guides with perturbations $\delta n^2(x,z)$ that can be factored as

$$\delta n^2(x,z)\ =\ \delta n^2(x)\ \cdot f(z)\ . \tag{11}$$

We shall first assume that the input pulse is Gaussian and that only one incident mode i is excited

$$E_y^0(\vec{r},t) = e^{i\omega_0 t\ -\ (t-t_0)^2/2\tau^2}\ u_i(x)e^{-i\beta_i z}\ \cdot N_\tau \tag{12}$$

where N_τ is a normalization factor for the input pulse. If input pulses are normalized to have equal energy, e.g.

$$\int E_y^0(x,z,t)^*\ E_y^0(x,z,t)\ dx\ dt\ =\ 1 \tag{13}$$

the normalization factor will be given by

$$N_\tau\ =\ \tau^{-1/2}\ \pi^{-1/4}. \tag{14}$$

To calculate the scattered pulse we decompose the initial pulse into its Fourier components (taking $t_0 = 0$)

$$E_y^0(\vec{r},\omega) = \frac{1}{2\pi} \int e^{-i\omega t}\ E_y^0(\vec{r},t)dt = \frac{e^{-(\omega-\omega_0)^2 \tau^2/2}}{\sqrt{2\pi}}\ \tau u_i(x)\ e^{-i\beta_i z}\ N_\tau \tag{15}$$

and propagate each frequency component ω with the GF $G(\vec{r}\ \vec{r}';\omega)$. Using equation(10)and approximating $G(\vec{r}\ \vec{r}';\omega)$ to lowest order by $G^0(\vec{r},\ \vec{r}';\omega)$, the scattered pulse can be expressed as

$$\delta E_y(\vec{r},t) = \iiint e^{i\omega t} \, d\omega \; \frac{\omega^2}{2ic^2} \; \sum_n \; \frac{1}{\beta_n} \; u_n^*(x') \, u_n(x) \; e^{-i\beta_n|z-z'|}$$

$$\cdot \delta n^2(x) f(z') \frac{e^{-(\omega-\omega_0)^2\tau^2/2}}{\sqrt{2\pi}} \tau u_i(x') \; e^{-i\beta_i z'} \; N_\tau \; dx' \, dz'. \tag{16}$$

Expanding each $\beta_n(\omega)$ around the central frequency ω_0 as

$$\beta_n(\omega) \simeq \beta_n(\omega_0) + \frac{\partial\beta_n}{\partial\omega}\Big|_{\omega_0} \cdot (\omega-\omega_0) + \ldots \tag{17}$$

$$= \beta_n^0 + v_n^{-1} \cdot (\omega-\omega_0) + \ldots$$

and retaining only $\beta_n(\omega_0)$ and the first derivative term

$$\frac{\partial\beta_n}{\partial\omega}\Big|_{\omega_0} = v_n^{-1} \tag{18}$$

where v_n is the modal group velocity, the expression for the scattered wave δE_y can be written as

$$\delta E_y^{\mp} \simeq \sum_n e^{i\omega_0 t \pm i\beta_n^0 z} \int e^{i(\omega-\omega_0)t} \; \frac{e^{-(\omega-\omega_0)^2\tau^2/2}}{\sqrt{2\pi}} \frac{\tau \omega_0^2}{2ic^2}$$

$$e^{\pm iv_n^{-1}(\omega-\omega_0)z} \; \frac{u_n(x)}{\beta_n^0} \cdot \varepsilon_{in} \cdot \eta(\beta_i \pm \beta_n) \; N_\tau \tag{19}$$

where ε_{in} and η are the transverse and longitudinal matrix elements of the perturbation given by

$$\varepsilon_{in} = \int u_n^*(x) \left[\delta n^2(x)\right] u_i(x) \; dx \tag{20}$$

and

$$\eta(\beta_i \pm \beta_n) = \int_{-\infty}^{\infty} e^{-i(\beta_i \pm \beta_n)z} f(z)dz \qquad (21)$$

and where $\mp$ refer to backward and forward scattered waves respectively.

The perturbations considered here lead in general to reflection, radiation loss, and mode-mixing. To obtain predictions of the backscattered OTDR signal, we must also account for several other sources of attenuation in the fiber such as Rayleigh scattering, intrinsic and extrinsic absorption, and curvature radiation losses (to be discussed in section IIIb). All of the latter may be incorporated into the GF approach by allowing the propagation constant for each mode to have an imaginary part

$$\beta_n \rightarrow \beta_n - i\alpha_n/2 . \qquad (22)$$

proportional to the total attenuation

$$\alpha_n(z) = \alpha_n(z)_{RAYLEIGH} + \alpha_n(z)_{ABSORB} + \alpha_n(z)_{BEND}. \qquad (23)$$

The Rayleigh and absorption losses are nearly uniform throughout a given fiber while the curvature radiation loss, when applicable, is generally confined to a limited length of fiber.

III. MODEL CALCULATION OF OTDR FROM BENDS

In this section we apply the formalism of section II to predict the OTDR return from bends in fibers. For purposes of illustration we will simplify the calculation by utilizing as our model a step index planar guide with a perturbation consisting of a bent region (possibly containing multiple loops) extending from $z = a$ to $z = a+L$ with a bend radius of curvature R_o. Use of the planar geometry allows us to demonstrate the principal physical effects associated with OTDR from bent fibers with a minimum of mathematical complexity. The methods employed are easily generalized to circular fibers at the expense of more tedious calculation.

For definiteness we choose the following values of parameters for the unperturbed guide: refractive index of the core $n_1 = 1.51$; refractive index of the clad (assumed to be of infinite extent) $n_2 = 1.50$; core width $d = 10$ μm, center wavelength for the input pulse $\lambda_o = 1$ μm. With this choice of parameters there will be a total of seven bound modes.

For gentle bends ($R_o \gg d$) a bent section of guide may be considered as an equivalent straight guide[2] with a perturbation given by

$$\delta n^2(x) = 2 \times n_o^{\,2}(x)$$

$$f_o(z) = \frac{1}{R_o(z)} = \frac{1}{R_o} \theta(z-a) \, \theta(a+L-z). \tag{24}$$

For this case eqn. (19) yields

$$\delta E_y^{\mp}(\vec{r},t) \simeq \sum_n e^{i\omega_o t \pm i\beta_n z} \left[\frac{\omega_o^2}{2ic^2}\right] \varepsilon_{in} \, \frac{u_n(x)}{\beta_n} \, \frac{i}{\left[\beta_i \pm \beta_n\right]}$$

$$\times \left[e^{-\frac{1}{2}(t \mp \frac{a+L-z}{v_n} - \frac{a+L}{v_i})^2/\tau^2} \; e^{-i(\beta_i \pm \beta_n)(a+L)} \right.$$

$$\left. -e^{-\frac{1}{2}(t \mp \frac{a-z}{v_n} - \frac{a}{v_i})^2/\tau^2} \; e^{-i(\beta_i \pm \beta_n)a} \right] N_\tau \tag{25}$$

(where we have omitted writing the superscript "o" on β_n^o's). From this expression it can be seen that backward or forward scattered waves will appear to come from the front and rear of the perturbed region with appropriate time delays and phases.

The reason no scattered waves come from the interior of the perturbed region is that contributions to the scattered wave from the interior cancel out exactly leaving only the uncancelled front and rear contributions. In general scattered waves will be generated from within a perturbed region if the perturbation is not entirely uniform. On a microscopic scale such non-uniformity is essentially the mechanism which produces Rayleigh scattering. Inhomogeneities in this case are due to frozen in thermal fluctuations in

53

density and composition which result in fluctuations of the refractive index. A calculation of Rayleigh scattering can be carried out using the GF methods discussed above but will not be undertaken here.

When all processes have been included, the OTDR return from the bend will consist of backscattered Rayleigh radiation that has been diminished by curvature radiation and by localized radiation losses as the pulse transits the front and rear of the bend plus a "reflected pulse" that consists of backscattering into bound modes that will also appear to come from the front and rear of the bend. Due to the random nature of the frozen in fluctuations giving rise to Rayleight scattering, the reflected pulse and the Rayleigh backscattered pulse will not interfere. This may be seen by expressing the total backscattered power as

$$P^{(-)}_{TOT}(t) = \sum_n \frac{\beta_n}{\omega\mu_o} \int < | \delta E^{(-)}_n(x,z,t) + \delta E^{(-)}_n{}_{FLT}(x,z,t) | >_{AV} dx$$

$$= P^{(-)}_{REF}(t) + \sum_n \frac{\beta_n}{\omega\mu_o} \int \delta E^{(-)*}_n(x,z,t) < \delta E^{(-)}_n{}_{FLT}(x,z,t) >_{AV} dx + c.c.$$

$$+ \sum_n \frac{\beta_n}{\omega\mu_o} \int < | E^{(-)}_n{}_{FLT}(x,z,t) |^2 >_{AV} dx. \qquad (26)$$

Since the thermal average of $\delta E^{(-)}_n{}_{FLT}$ is zero, contributions to the OTDR backscattered pulse from Rayleigh scattering and from the reflected pulse will be simply additive

$$P^{(-)}_{TOT}(t) = P^{(-)}_{REF}(t) + P^{(-)}_{RAYL}(t) \qquad (27)$$

In the following sections we will discuss each of these contributions separately. In section IV numerical results using the above model for various curvature radii and pulse lengths will be discussed.

IIIa. TRANSITION LOSS

The relative power that is radiated away as the input pulse passes the perturbed region can be calculated as

$$\frac{\delta P_{TR}(t)}{P_0} = \int_0^{n_2 k_0} d\beta_k \left[\frac{\delta P_k^+ + \delta P_k^-}{P_0} \right] \tag{28}$$

where

$$\delta P_k^{\pm}/P_0 = \frac{1}{P_0} \int dx \, \delta E_y^{\pm}(k) \frac{i}{\omega\mu_0} \frac{\partial}{\partial z} \delta E_y^{\pm *}(k) \tag{29}$$

are the forward and backward radiation losses and $\delta E_y^+(k)$ is the integrand of eqn. (25) for the continuum contributions. Due to the denominator $(\beta_i \pm \beta_k)^{-1}$ in eqn. (25) backward radiation will be much smaller than forward radiation and can be neglected. Using the expression for $\delta E_y^+(k)$ for forward scattering from eqn. (25) and performing the x integration then yields

$$\frac{\delta P_{TR}(t)}{P_0} = \frac{k_0^4}{4\beta_i} \int_0^{n_2 k_0} d\beta_k \frac{|\epsilon_{ik}|^2}{(n_2^2 k_0^2 - \beta_k^2)^{\frac{1}{2}} (\beta_i - \beta_k)^2}$$

$$\times \left[f_{ik}^2 + g_{ik}^2 - 2 f_{ik} g_{ik} \cos((\beta_i - \beta_k)L) \right] \tag{30}$$

where $f_{ik} = e^{-\left[t - (a-z)v_k^{-1} - av_i^{-1}\right]^2 / 2\tau^2} \cdot N_\tau$

and $g_{ik} = e^{-\left[t - (a+L-z)v_k^{-1} - (a+L)v_i^{-1}\right]^2 / 2\tau^2} \cdot N_\tau \tag{31}$

represent the radiation pulses coming from the front and rear of the bend.

If we consider the L dependence of the forward radiation loss, there are two limiting regimes. In the first $L \gg (\beta_i - \beta_k)^{-1}$ for all β_k in the range $n_2 k_0 > \beta_k > 0$. For this case the rapidly oscillating cross term pro-proportional to $\cos((\beta_i - \beta_k)L)$ can be set equal to zero and the forward radiation can be considered as being lost in two steps, the first as the pulse transits the beginning of the bend at z=a and the second as it passes the end of the bend at z=a+L. For this case (after factoring out the bracketed term representing the pulse shape) the transition loss T_i is given by

$$T_i = \frac{k_0^4 n_2 k_0}{4\beta_i} \int_0^{n_2 k_0} \frac{d\beta_k}{(n_2^2 k_0^2 - \beta_k^2)^{\frac{1}{2}}} \frac{|\epsilon_{ik}|^2}{(\beta_i - \beta_k)^2} \tag{32}$$

In the second regime $L(\beta_i - \beta_k)^{-1} \lesssim 10^2 - 10^3$ the cross term may not be neglected and there is the possibility of radiation fields from the front and back of the bend interfering. For this case $f_{ik} \sim g_{ik}$ and the integration over all radiation modes is given by

$$2T_i = \frac{k_0^4}{4\beta_i} \int_0^{n_2 k_0} d\beta_k \frac{|\epsilon_{ik}|^2}{\rho_k (\beta_i - \beta_k)^2} \cdot 2(1 - \cos((\beta_i - \beta_k)L))$$

$$= \frac{k_0^4}{4\beta_i} \int_0^{n_2 k_0} d\beta_k \left[\frac{4 \sin^2((\beta_i - \beta_k)\frac{L}{2})}{(\beta_i - \beta_k)^6} \right] \left[\frac{16\Delta^4 \cos^2 \kappa_i d \, \sin^2 \sigma_i d \, N_e^2 \rho_k}{(\beta_i + \beta_k)^4 \pi \left[\rho_k^2 \sin^2 \sigma_k d + \sigma_k^2 \cos^2 \sigma_k d \right]} \right]$$

with

$$\rho_k^2 = (n_2^2 k_0^2 - \beta_k^2), \sigma_k^2 = (n_1^2 k_0^2 - \beta_k^2), \kappa_i^2 = (n_1^2 k_0^2 - \beta_i^2)$$

$$\Delta^2 = k_0^2 (n_1^2 - n_2^2), N_e = (d + \gamma_n^{-1})^{-1/2},$$

$$\gamma_n = (\beta_n^2 - n_2^2 k_0^2)^{1/2}. \tag{33}$$

An approximate value for this integral may be obtained by assuming that the slowly varying second factor ($\equiv F$) can be taken to be roughly constant over the region where the first factor is a maximum ($\beta \sim \beta^* \sim n_2 k_0$). With this assumption we obtain an upper bound for the transition loss

$$2T_i \sim \frac{k_0^4}{4} \frac{\pi}{2\cdot 5!} \left[\frac{105}{32} \delta_i^{-9/2} - A(1 - C_2(\delta_i L) - S_2(\delta_i L)) \right.$$

$$-B(C_2(\delta_i L) - S_2(\delta_i L)) - C_e (\sin(\delta_i L) + \cos(\delta_i L)) +$$

$$\left. C_0(\sin(\delta_i L) - \cos(\delta_i L)) \right] \cdot F(\beta^*) \qquad (34)$$

where $\qquad \delta_i = \beta_i - n_2 k_0$, C_2 and S_2 are Fresnel integrals, and

$$A = 105/32 \, \delta_i^{-9/2} - {}^{15}/4 \, L^2 \, \delta_i^{-5/2}$$

$$+ 5/2 \, L^4 \, \delta_i^{-1/2}$$

$$B = -75/16 \, L \, \delta_i^{-7/2} + 5/2 \, L^3 \, \delta_i^{-3/2} + L^5 \, \delta_i^{1/2}$$

$$C_e = L^{1/2}/\sqrt{2\pi} \, (105/16 \, \delta_i^{-4} - 3L^2 \, \delta_i^{-2} - L^4)$$

$$C_0 = L^{1/2}/\sqrt{2\pi} (5L \, \delta_i^{-3} - 2 \, L^3 \, \delta_i^{-1}). \qquad (35)$$

For the waveguide we have chosen as an example the δ_i's are of the order $\delta_i \sim 10^4 \, m^{-1}$. The dependence of T_i on mode number will thus be given roughly by $T_i \sim \delta_i^{-9/2}$.

The calculation of transition loss given above is idealized to the extent that we have assumed an infinite cladding. For a finite clad any radiation that leaves the core region is effectively absorbed locally. The transition loss formula without the interferences term given by eqn. (25) would thus be more appropriate. Likewise the assumption of the bent guide as an equivalent straight guide obscures the fact that a guide may satisfy

57

the condition for interference to be important while the front of the bend may be topologicaIly "far" from the rear of the bend due to looping. An additional constraint that $L << R_0$ should thus be imposed to further limit the domain where the interference term is important.

IIIb OTDR FROM BENDS INCLUDING CURVATURE LOSS

Before the Rayleigh scattering contribution to the OTDR return can be obtained for bend perturbations, we must first incorporate an additional loss mechanism due to curvature radiation (tunneling loss) that is not accounted for within lowest order GF theory and that must be specifically included in the imaginary part of each propagation constant β_n. The origin of this curvature loss is discussed below.

If we view the refractive index profile as a quantum mechanical potential $V_{(x)} = -k_0^2 n^2(x)$ then the perturbation $\delta V^2 = -k_0^2 \frac{x}{R} n_0^2(x)$ will transform the step index potential as indicated in fig. 1.

It can be seen that all of the former bound states now have the possibility of tunneling through the lowered potential carrier to continuum states and calculation of this tunneling rate will yield a curvature loss α^i_{RAD} proportional to

$$e^{-\frac{2}{3} R\gamma_i^3 / \bar{\beta}^2} \quad \text{where } \gamma_i^2 = \beta_i^2 - n_2^2 k_0^2 \text{ and } \bar{\beta} = n_1 k_0. \tag{36}$$

Including both the curvature loss and the transition loss, the total backscattered signal due to Rayleigh scattering can be calculated for one incident mode $\underline{i}$ as

$$\frac{P^{(-)}}{P_0}_{\text{RAYLEIGH}} = \alpha_{\text{RAYLEIGH}} \cdot \xi \cdot \int_{\infty}^{\infty} e^{-(t-(z'-z)/v_i - z'/v_0)^2/\tau^2} \tag{37}$$

$$\times \left\{ \theta(a-z') \exp(-2\alpha_{\text{TOT}}z') \right.$$

$$+ (1-T_i-R_i)\left[\theta(z'-a)\theta(a+L-z') \right] e^{-2\alpha_{\text{TOT}}z'} e^{-2\alpha^i_{\text{RAD}}(z'-a)}$$

$$\left. + (1-T_i-R_i)^2 \theta(z'-(a+L)) \; e^{-2\alpha_{\text{TOT}}z'} \; e^{-2\alpha^i_{\text{RAD}} \cdot L} \right\} dz'$$

where T_i and R_i are the transition loss and reflected power for the ith mode, where

$$\alpha_{\text{TOT}} = \alpha_{\text{ABSORB}} + \alpha_{\text{RAYLEIGH}} \tag{38}$$

are taken to be independent of mode number,

and α^n_{RAD} is given for the step index guide [4] as

$$\alpha^n_{\text{RAD}} = \frac{\gamma_n^2}{\beta_n(1+\gamma_n a)} \frac{\kappa_n^2}{(n_1^2-n_2^2)k_0^2} e^{2\gamma_n a} \; e^{-2/3(\gamma_n^3/\beta_n^2)R} \tag{39}$$

with

$$\xi = \frac{3}{8} \frac{(n_1^2-n_2^2)}{n_1^2} \tag{40}$$

a geometrical factor to approximate the fraction of Rayleigh scattered power that is backscattered into the guide [5]. The integrals appearing in this expression can all be expressed analytically in terms of error functions.

From the expression (39) for α_{RAD}^n it can be seen that the curvature loss depends exponentially upon both R_0 and the mode number n. The step index guide we have chosen as an example yields $(\gamma_6)^3 \sim (\gamma_0)^3/12$; tunneling losses for the weakly bound modes can thus be many orders of magnitude greater than those of tightly bound modes.

IIIc DIRECT REFLECTIONS AND EFFECTS DUE TO GRADUAL BEND ONSET

Due to mechanical stiffness, the transition from a straight guide to a curved section of guide will not, in general, occur abruptly, but will change gradually over some finite distance $\delta = 2\pi/q$ as indicated in fig. 2. In this subsection we consider the effect of a continuous transition region (curvature radius changes from $R^{-1}=0$ to $R^{-1} \neq 0$ over a finite distance) on the OTDR return.

We first consider a transition model with

$$R^{-1}(z) = \frac{1}{2}\left[th(q(z-a))+th(q(a+L-z))\right] \tag{41}$$

which yields for the longitudinal matrix element

$$\eta(p_\pm) = \int_\infty^\infty R^{-1}(z)\, e^{-ip_\pm z}\, dz$$

$$= i\; e^{-ip_\pm a}\left[e^{-ip_\pm L}-1\right]\left\{\frac{\pi}{q}\;\frac{sh\,(p_\pm \pi/2q)}{[ch(p\pm \pi/q)-1]}\right\} \tag{42}$$

where $p_\pm = \beta_i \pm \beta$. In the point limit $\delta \to 0$, $\eta \to \eta_0$, where

$$\eta_0(p_\pm) = \frac{i}{p_\pm}\, e^{-ip_\pm a}\left[e^{-ip_\pm L}-1\right] \tag{43}$$

is the longitudinal matrix element used in eqn. (25) For the case of backward scattering where $q \ll p_\pm$, eqn. (42) yields

$$n(p_+) \simeq i \, e^{-ip_+ a} \left[e^{-ip_+ L} -1 \right] \frac{\pi}{q} \, e^{-p_+ \pi/2q}$$

$$=n^0(p_+) \left[\frac{p_+ \pi}{q} \, e^{-p_+ \pi/2q} \right] \tag{44}$$

which goes to zero exponentially, suppressing reflected waves. Only if $\delta < \lambda_0$ will backward scattered waves be significant. For forward scattering it is possible for q to be comparable with p_- (for the guide of section III, $q = p_- \sim 10^4 \Rightarrow \delta \sim 2\pi \times 100 \ \mu m$) in which case n can be of the same order as n_0.

In a second model[6] for the transition we take

$$\frac{1}{R_{(z)}} = \begin{cases} \dfrac{1}{R_0} \dfrac{(1-\cos(q(z-a)))}{2} , & a < z < a + \pi/q \\[4mm] \dfrac{1}{R_0}, & a + \pi/q < z < a + L - \pi/q \\[4mm] \dfrac{1}{R_0} \dfrac{(1-\cos(q \ (a+L-z)))}{2}, & a+L - \pi/q < z < a+L \end{cases} \tag{45}$$

yielding

$$n(p) = \frac{e^{-ipa}}{2R_0} \frac{q^2}{ip(p^2-q^2)} \left[e^{-ipL}(1+e^{ip\pi/q}) \right.$$

$$\left. -(1 + e^{-ip\pi/q}) \right] \tag{46}$$

which has the same q→∞ point limit as the first model. For backward scattering and $q \ll p_+$, the overall magnitude of $n(p_+)$ is down by a factor q^2/p_+^2 over $n_0(p_+)$, yielding a drastically reduced reflected pulse. For the reflected pulse to be of the same order as the Rayleigh backscattered pulse, δ would have to be of the same order as λ_0, i.e. smaller than the width of the guide.

61

If the second model is changed to allow a uniform series of a sinusoidal bends ie.,

$$\frac{1}{R(z)} = \frac{1}{R_0} \frac{(1-\cos q(z-a))}{2} \ , \ a < z < a \ + \ \frac{2N\pi}{q}$$

$$N = 1, 2, 3...$$

(47)

we find

$$\eta(p) = e^{-ipa} \ (e^{-ip2\pi N/q} -1)\frac{q^2}{ip \ (p^2-q^2)}$$

(48)

which for N=1 agrees with the second model when $L = 2\pi/q$ and is similar in

form to the single bend of the second model for N>1.

IV   COMPUTED RESULTS

To illustrate the effects of bend radius of curvature and pulse length
on OTDR returns as calculated for the model of section III, we have plotted
in figs. 3 through 10 the OTDR return pulse vs. time for bends having curvature radii of 10 cm and .56 cm, and pulse widths of 10 ns and 100 ns.
For these curves we have taken the longitudinal matrix element to be $\eta = \eta_0$
and have assume^d reflections to be zero. The bend length L and the position
of the bend onset a have been taken to be L = 3.5m and a = 10 m respectively.

62

The scattering coefficient for Rayleigh scattering and the absorption coefficient for impurity absorption have been taken as $\alpha_{RAYLEIGH}$ = .77 db/km and α_{ABSORB} = .54 db/km respectively. For figures 3 through 6 the waveguide is assumed to be "uniformly" illuminated with an input field given by

$$u_{in} = \frac{1}{2} \; (u_0(x)+u_2(k)+u_4(x)+u_6(x))$$

$$= \sum_i a_i \, u_i$$

with $\qquad \begin{cases} a_i = 1/2, \; i \text{ even} \\ \\ a_i = 0, \; i \text{ odd} . \end{cases}$ $\qquad\qquad$ (49)

The inclusion of more than one input mode in eqn. (49)leads to a modification of eqn. (28) which represented the transition loss for one input mode, that includes new cross terms

$$\frac{P_{TR}(t)}{P_0} = \frac{k_0^4}{4\overline{\beta}_{in}} \int_0^{n_2 k_0} \frac{d\beta_k}{(n_2^2 k_0^2 - \beta_k^2)^{\frac{1}{2}}} \sum_{i,j} \frac{\varepsilon_{ik}\varepsilon_{jk}^* \, a_i a_j}{(\beta_i - \beta_k)(\beta_j - \beta_k)}$$

$$\times \left\{ \left[f_{ik}^2 + g_{ik}^2 - 2 f_{ik}g_{ik} \cos(\beta_i - \beta_k) L \right] \delta_{ij} \right.$$

$$+ (1-\delta_{ij}) \left[f_{ik}f_{jk} \cos(\beta_i - \beta_j)a + g_{ik}g_{jk} \cos(\beta_i - \beta_j)(a+L) \right.$$

$$- f_{ik}g_{jk} \cos((\beta_i - \beta_k)a - (\beta_j - \beta_k)(a+L))$$

$$\left. \left. - f_{jk}g_{ik} \cos((\beta_j - \beta_k)a - (\beta_i - \beta_k)(a+L)) \right] \right\} . \qquad (50)$$

where $\overline{\beta}_{in} = (\beta_0 + \beta_2 + \beta_4 + \beta_6)/4$.

For the off-diagonal terms in eq. (50) to be important the wave packets for each pair of modes, as given by eqn.(31) must overlap. If the onset length a is large and the group velocities for the various modes are different enough, the overlap products will be very small. In order to keep the present calculation as simple as possible we have assumed that the length a and the dispersion in group velocities are large enough to enable the off-diagonal terms be neglected.

Figures 3 and 4 indicate the behavior of the OTDR return for the case $R_o = 10$ cm where transition loss is the dominant loss mechanism. In figure 3 the pulse width = 10 ns is smaller than the temporal extent of the bend $t_b = \frac{2L}{v_o} = 35$ ns while in figure 4 the pulse width is larger (we note that since the abscissa represents the round trip time, the front and rear of the bent section appear at t = 100 ns and t = 135 ns).

Since the return pulse behaves roughly as $P \propto e^{-\alpha_{eff} Z}$ we have also plotted the derivative of this curve to indicate an effective loss rate α_{eff}. The curve for α_{eff} in figure 3 illustrates the transition loss from the front and rear of the bend for $\tau < t_b$.

Figures 5 and 6 illustrate the case of uniform illumination for $R_o = .56$ cm where curvature radiation is the dominant loss mechanism. Since the input power is equally distributed over the four symmetric modes while the outermost modes 4 and 6 can radiate their power away over a very short distance, approximately half of the input power ($\sim$3db) is lost in a very short time after passing the onset of the bend if the pulse width is small (fig. 5, τ= 10 ns) or over a proportionately longer time for longer pulses (fig. 6, τ= 100 ns). (We note that the extra wiggles in the curves for α_{eff} in figures 5 and 6 are an artifact due to numerical differentiation and would be absent in a more exact evaluation).

To illustrate the dependence of transition loss and curvature radiation loss on mode number we have plotted in figures 7 through 10 the OTDR return from the model guide of section III excited by a pulse consisting of equal weights of

$$u_0 \text{ and } u_2 \quad \text{(curve A)}$$

$$u_2 \text{ and } u_4 \quad \text{(curve B)}$$

$$u_4 \text{ and } u_6 \quad \text{(curve C).}$$

For the case of R_0 = 10 cm, shown in figures 7 and 8 where transition loss dominates, it can be seen that only the least tightly bound mode 6 encounters an appreciable transition loss at z=a and z=a+L. The case R_0 = .56 cm, where curvature radiation loss dominates, is shown in figures 9 and 10. Since

$\alpha_{6\ RAD} \sim 2.3 \times 10^3$ db/km, $\alpha_{4\ RAD} \sim 1.4 \times 10^4$ db/km, and $\alpha_{2\ RAD} \sim .2$ db/km, only the two outermost modes are affected to an appreciable extent. Mode 6 is lost entirely within a very short distance ($\sim 10^{-5}$m) while mode 4 is only fractionally depleted in traversing the bend. The sharp dropoff in curve C of figs. 9 and 10 at

t = 100 ns is due to the rapid loss of mode 6 input power.

In figures 11 and 12 we have illustrated the OTDR return for the case where $\eta = \eta_0$ and reflected pulses are not suppressed.

V CONCLUDING REMARKS

We have presented a theory of OTDR from weak static perturbations in optical fibers, utilizing a time-dependent Green's function formulation. The formulae we have obtained incorporate the effects of direct reflection and transition loss. The theory also incorporates uniform attenuation from absorption and scattering, as well as curvature radiation losses (when applicable). We have applied the theory to examine the OTDR signal (and its time derivative) from fiber bends as a function of bend length and radius, and the dependence on mode number and pulsewidth.

Our calculations for a simplified slab guide model demonstrates that transition losses dominate for large radius bends, while curvature losses dominate for small radius bends. In either case, if the spatial pulse width is much larger than the length of the bent region, the loss shows up as a single drop in the OTDR signal. As expected, the size of the loss is very sensitive to mode number. When the pulse width is short compared to the bent region, separate features due to the front and end of the bend may be observed in certain instances. Moreover, if the bend region occurs abruptly, then peaks due to reflections can be observed in OTDR with short pulses. If the bend onsets gradually, however, then reflection effects will be suppressed.

Experiments to date have indicated agreement with several general features mentioned above, such as the overall loss at the bend and the sensitivity on the spatial mode patterned launched in the fiber. However, further refinements in both the theoretical model (extension to circular fibers) as well as the experimental techniques (better signal-to-noise ratio, availability of shorter pulses) are required before a quantitative comparison between theory and experiment can be carried out.

REFERENCES

1)   M.D. Rourke, S.M. Jensen, and M.K. Barnoski, in "Fiber Optics,
     Advances in Research and Development" (Plenum, N.Y., 1979);
     M.D. Rourke, this volume.

2)   M. Sodha and A. Ghatak, "Inhomogeneous Optical Waveguides" (Plenum,
     N.Y., 1977) Chap. 8.3.

3)   D. Marcuse, "Field deformation and loss caused by curvature of
     optical fibers", J. Opt. Soc. Am., 66 311 (1976).

4)   D. Marcuse, "Light Transmission Optics" (Van Nostrand Reinhold, N.Y.,
     1972).

5)   M.D. Rourke, Optics Comm., "Maximum achievable crosstalk isolation in
     full-duplex single-strand fiber-optic systems", 25 40 (1978).

6)   W.A. Gambling, H. Matsumura, C.M. Ragdale, "Curvature and microbending
     losses in single mode optical fibers", Opt. Quant. Elec., 11, 43 (1979).
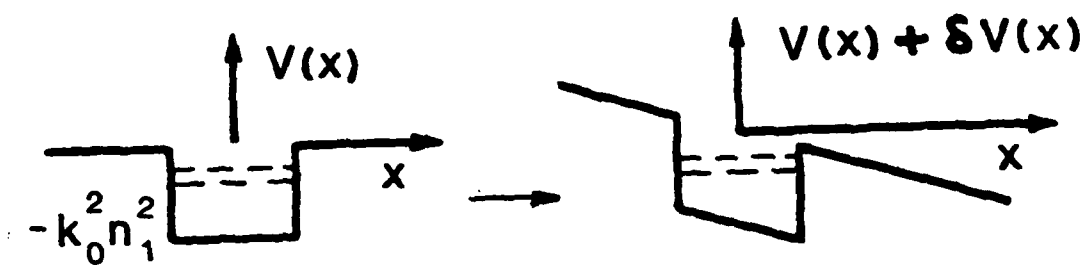
Fig. 1.   Effect of bend perturbation on waveguide "potential well".
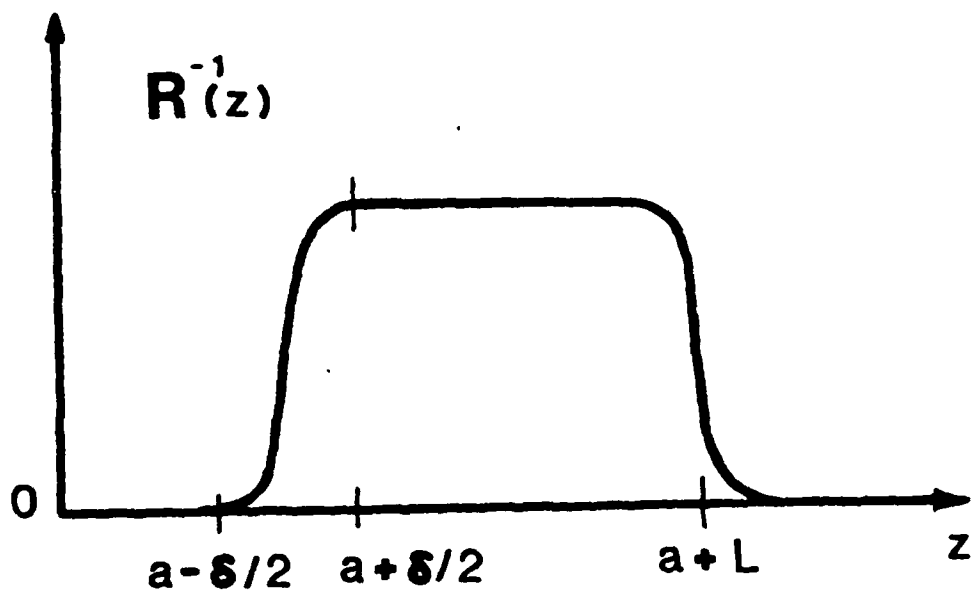
Fig. 2.   Inverse of curvature radius $R^{-1}(z)$ versus Z.

69
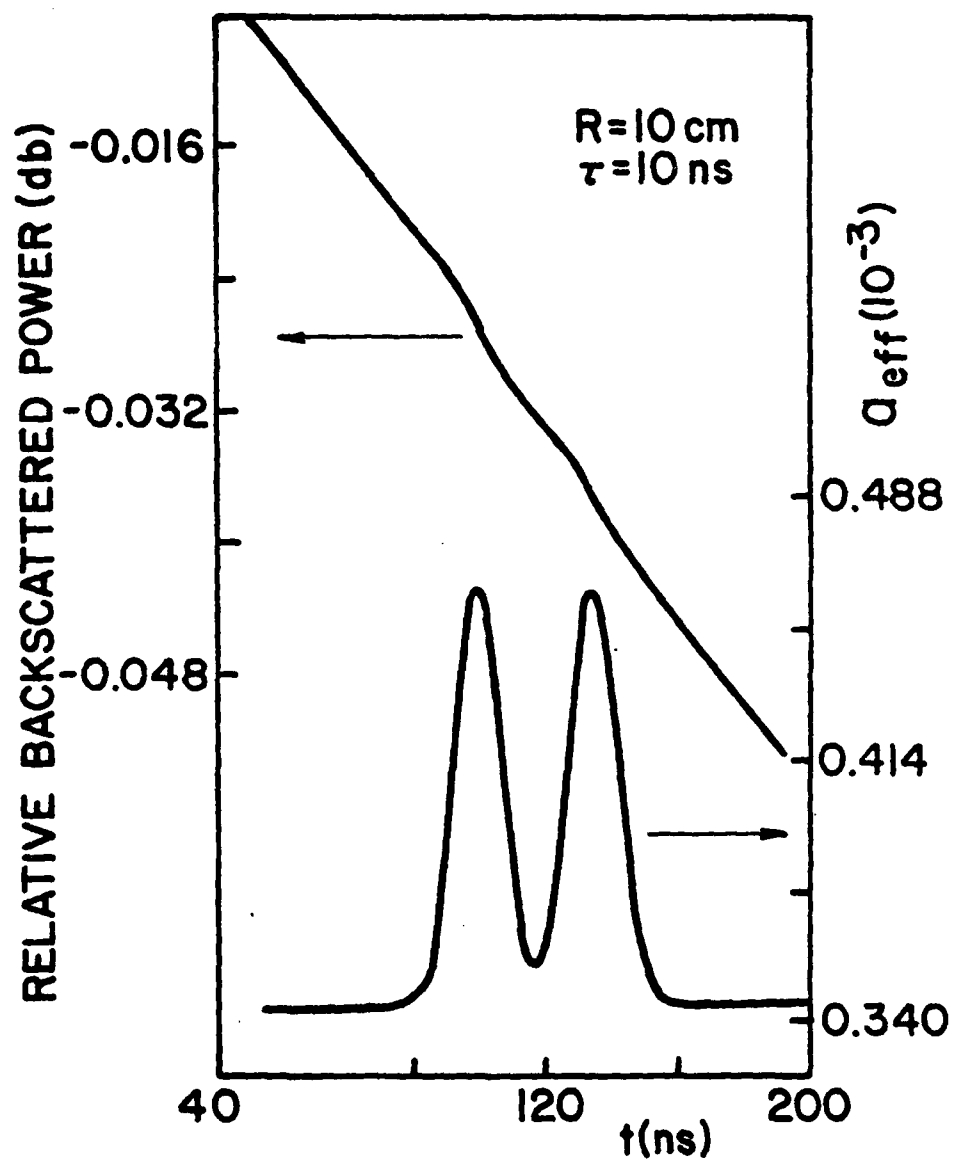
Fig. 3. Upper curve is the Log_{10} of the intensity of the OTDR return pulse versus time for "uniform excitation"; lower curve is the derivative of the upper curve in units of m^{-1} ($m^{-1} = 4.343 \times 10^3 \text{db/km}$).
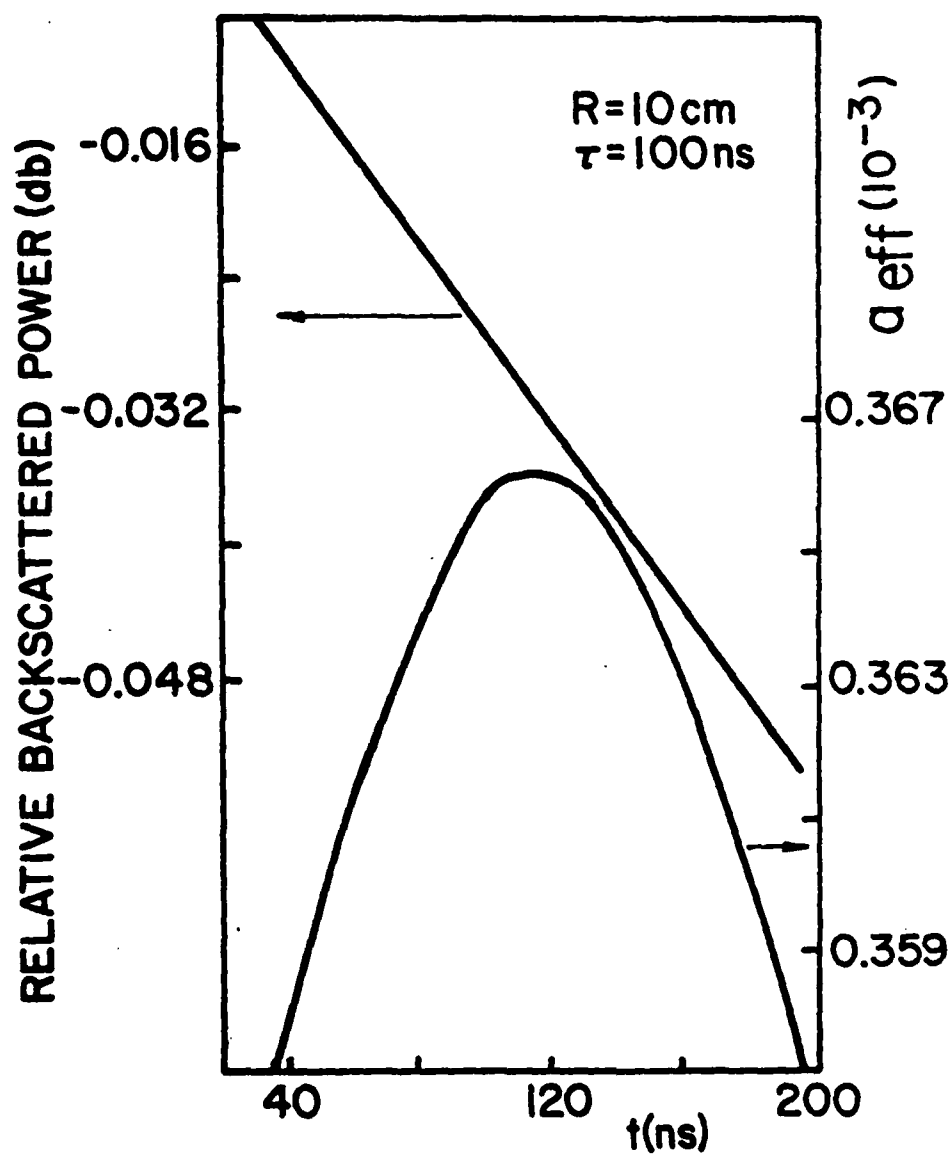
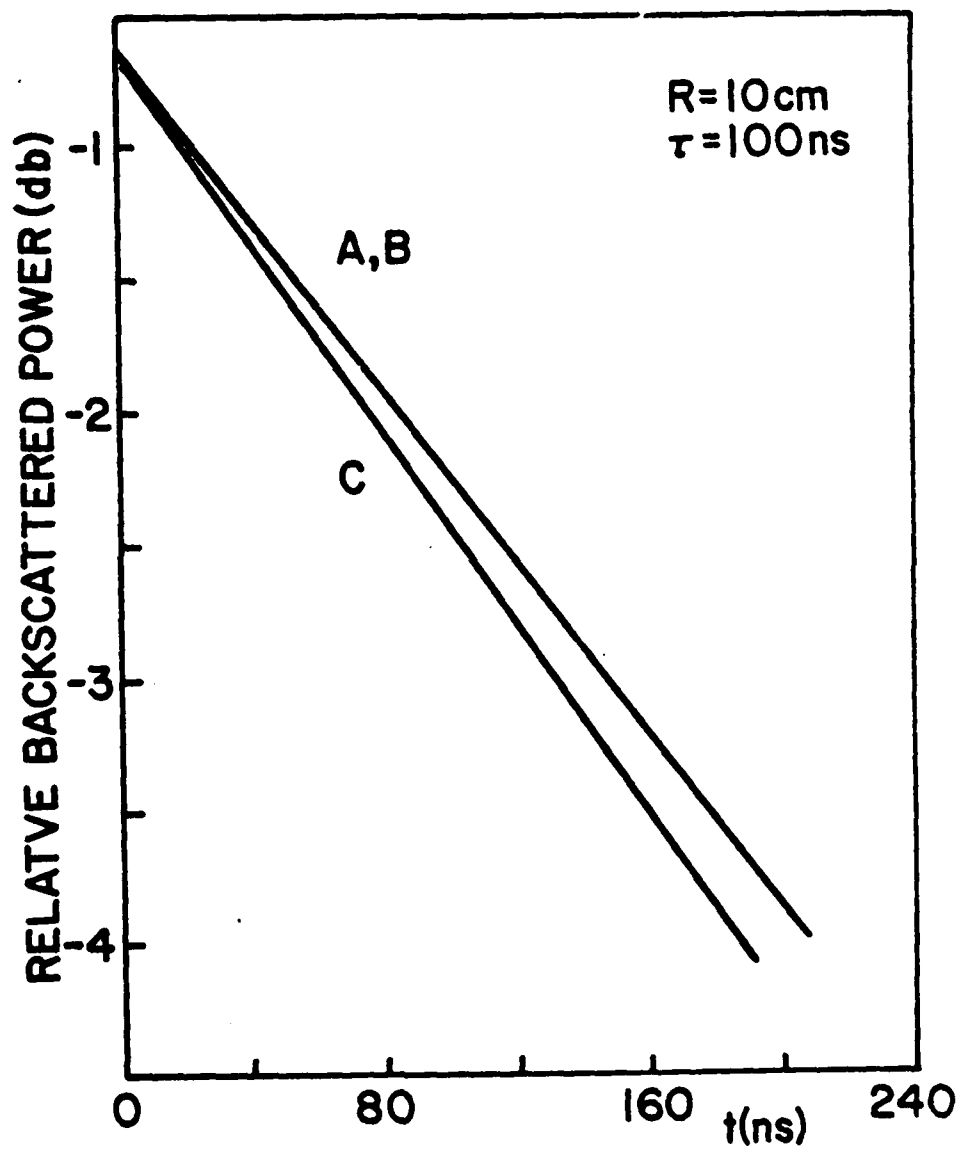Fig. 4.   Same as fig. 3, but for other choices of parameters.
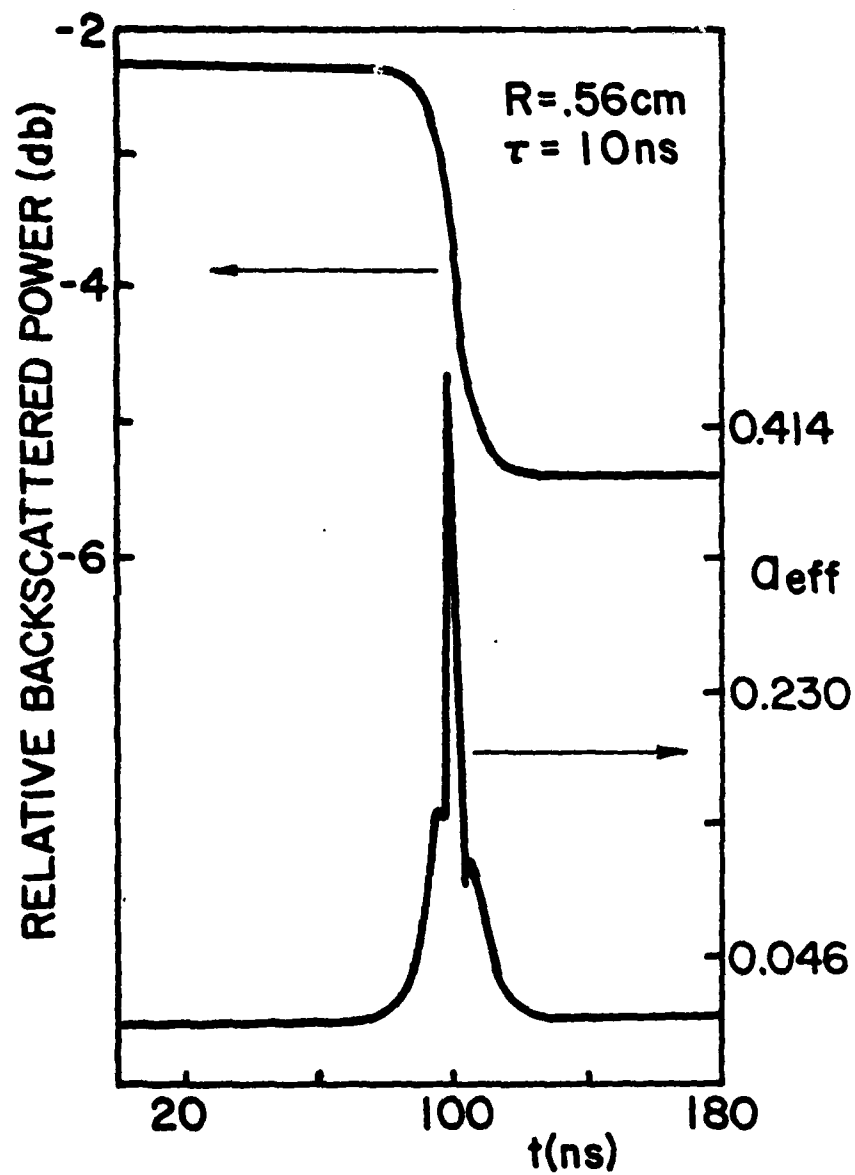
Fig. 5. Same as fig. 3, but for other choices of parameters.
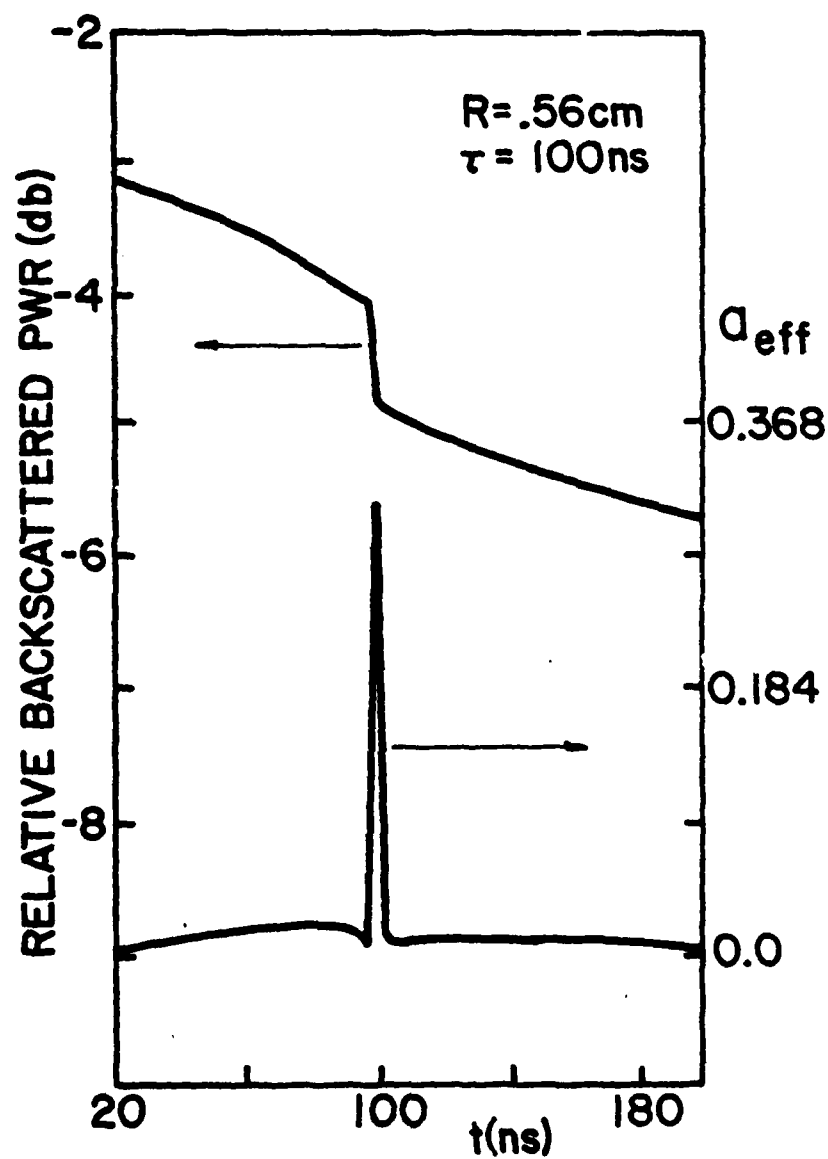
Fig. 6.   Same as fig. 3, but for other choices of parameters.

73
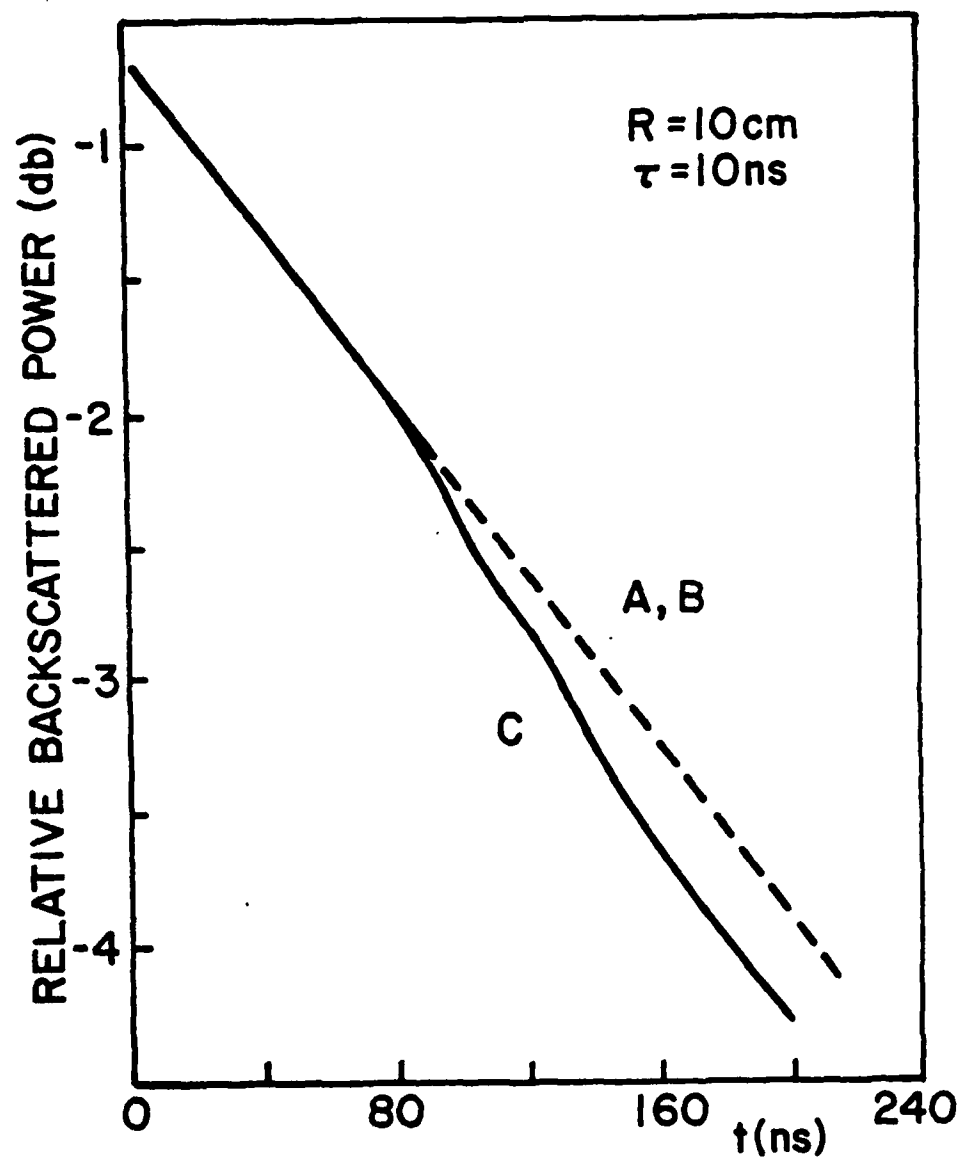
Fig. 7. Log$_{10}$ of the intensity of the OTDR return pulse vs time: Curve A
results from initial excitation of modes 0 and 2 (in units of
.016 db); Curve B, modes 2 and 4 (in units of .016 db); curve C,
modes 4 and 6 (in units of .016 db).

74

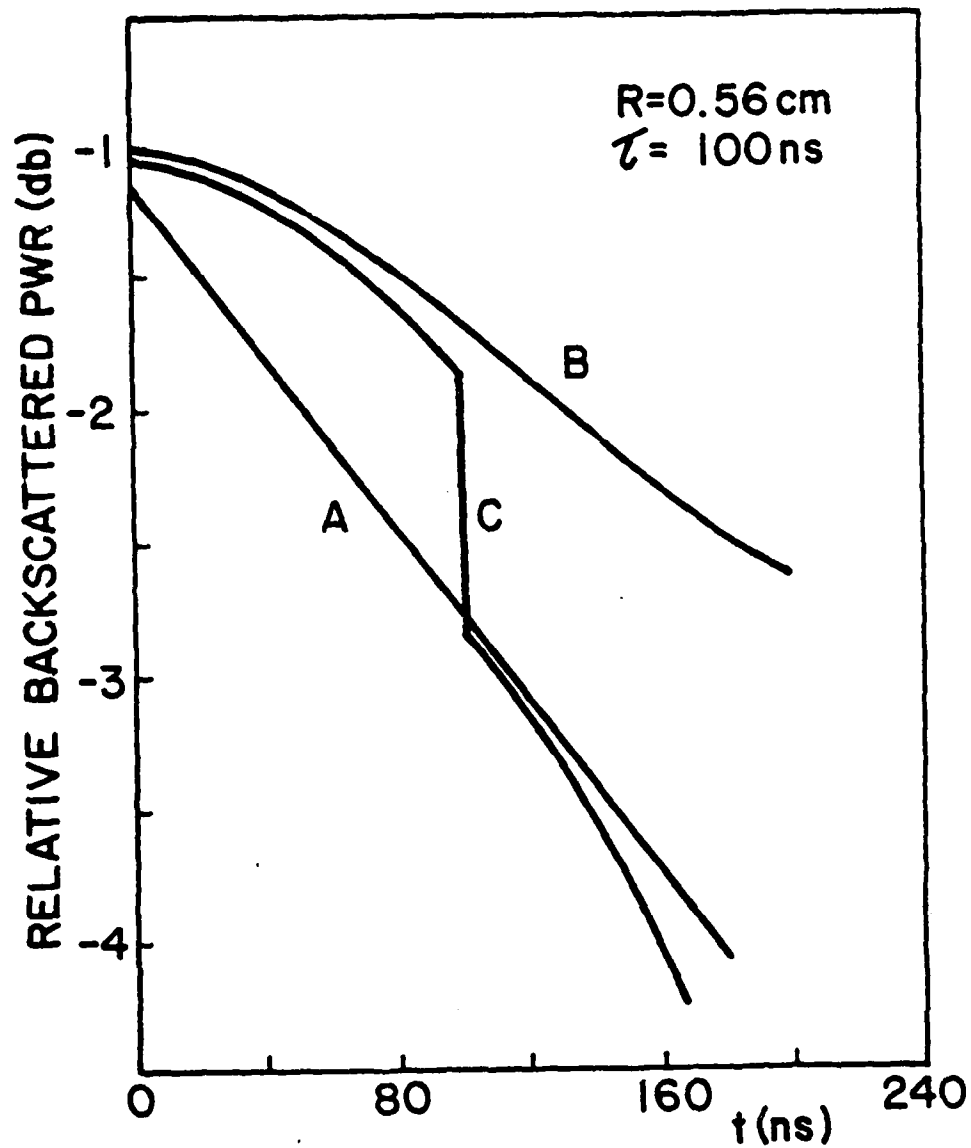Fig. 8.   Same as fig. 7, but for other choices of parameters.
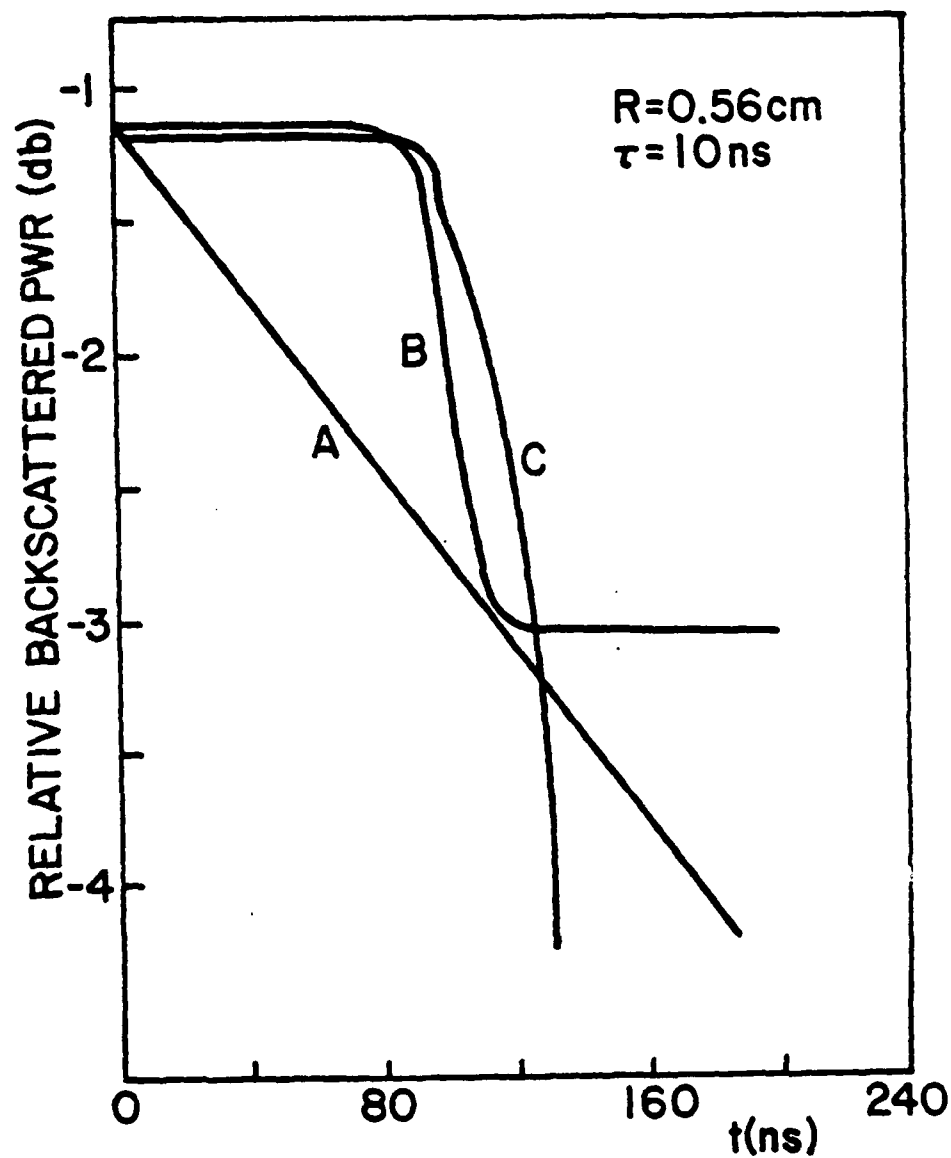
Fig. 9. Same as fig. 7, but for other choices of parameters. Also units are changed as follows:

curve A in units of .016 db, curve B in units of 1.6 db, curve C in units of 20. db.

76

Fig. 10.   Same as fig. 7, but for other choices of parameters. Also units are

changed as follows:

curve A in units of .016 db, curve B in units of 1.6 db,

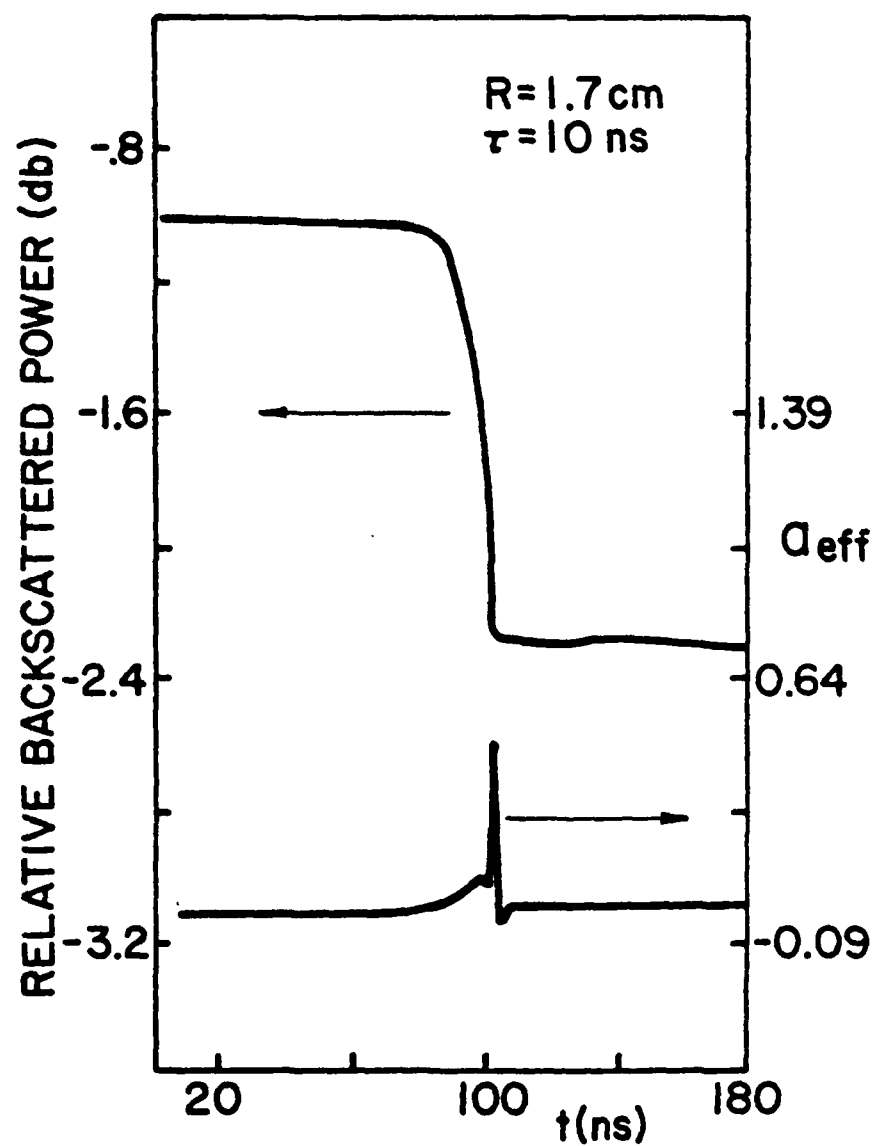curve C in units of 3.2 db.

77

Fig. 11. Same as fig. 3, but with direct reflection included (as well as other choices of parameters).
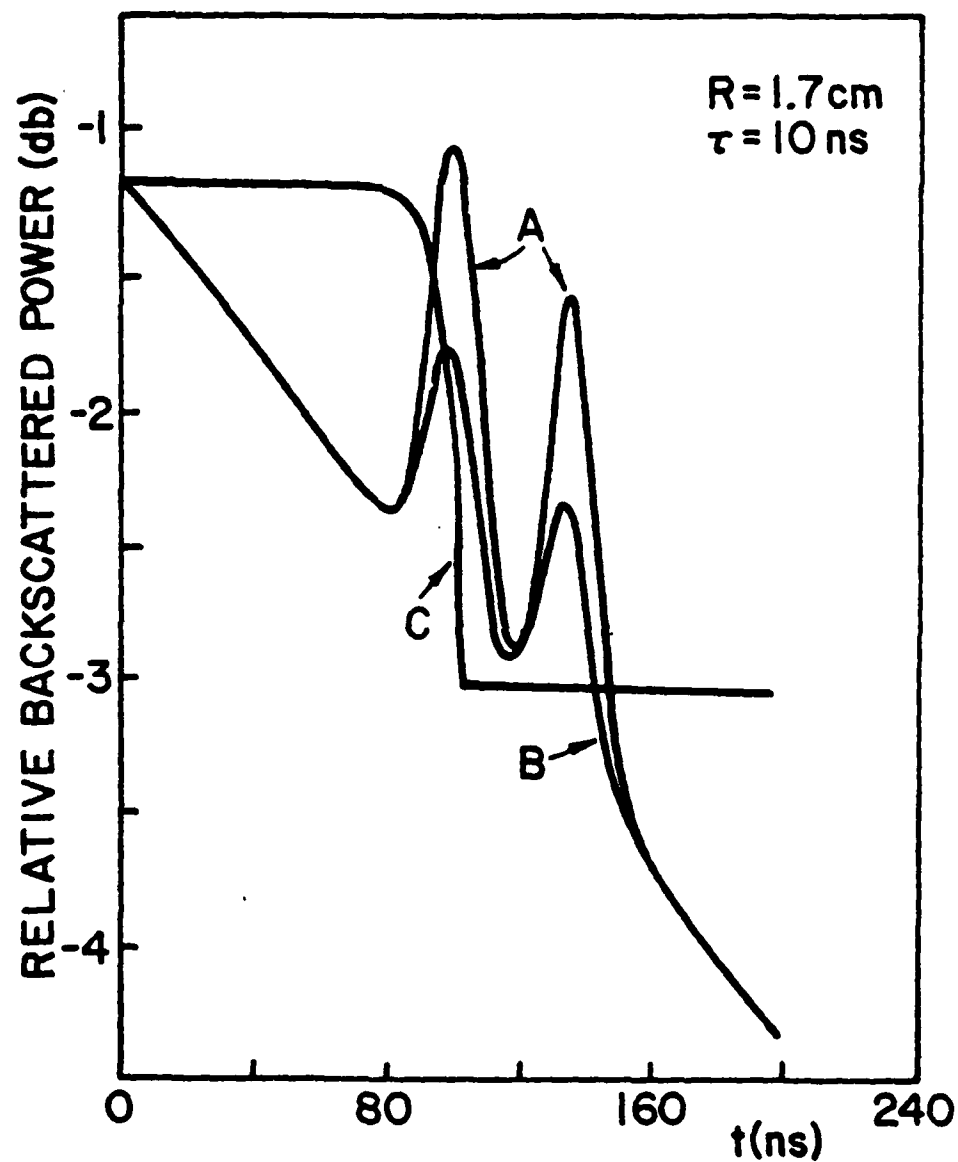
Fig. 12. Same as fig. 7 but with direct reflection included (as well as
other choices of parameters). Also units are changed as follows:
curves A and B in units of .016 db, curve C in units of 1.6 db.

79

MISSION
of
Rome Air Development Center

RADC plans and executes research, development, test and selected acquisition programs in support of Command, Control Communications and Intelligence (C^3I) activities. Technical and engineering support within areas of technical competence is provided to ESD Program Offices (POs) and other ESD elements. The principal technical mission areas are communications, electromagnetic guidance and control, surveillance of ground and aerospace objects, intelligence data collection and handling, information system technology, ionospheric propagation, solid state sciences, microwave physics and electronic reliability, maintainability and compatibility.

4-8